

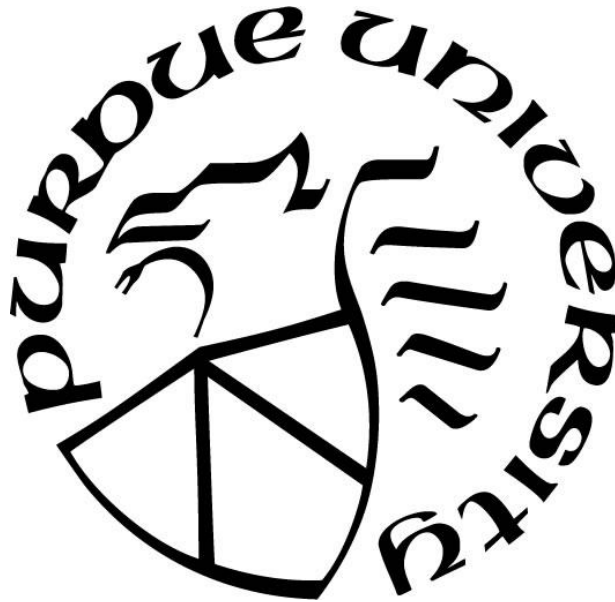
**DATA DRIVEN DENSE 3D FACIAL RECONSTRUCTION FROM 3D
SKULL SHAPE**

by
Anusha Gorrila

A Thesis

*Submitted to the Faculty of Purdue University
In Partial Fulfillment of the Requirements for the degree of*

Master of Science



Department of Computer and Information Sciences

Indianapolis, Indiana

August 2019

**THE PURDUE UNIVERSITY GRADUATE SCHOOL
STATEMENT OF COMMITTEE APPROVAL**

Dr. Mihran Tuceryan, Chair

Department of Computer and Information Sciences

Dr. Shiao-fen Fang

Department of Computer and Information Sciences

Dr. Jiang-Yu Zheng

Department of Computer and Information Sciences

Approved by:

Dr. Mihran Tuceryan

Head of the Graduate Program

This research is dedicated to my family and friends

ACKNOWLEDGMENTS

I would like to take this opportunity to thank Dr. Mihran Tuceryan, my faculty advisor for his constant support and guidance throughout my time here at Indiana University Purdue University, Indianapolis (IUPUI). I believe that he is one of the nicest and humble persons to come across and it would not have been possible for me to have completed this research without his day to day help.

I would also like to thank Dr. Jiang Yu Zheng and Dr. Shiaofen Fang for agreeing to be a part of my Thesis committee. It is an honor for me indeed. In general, I would like to thank the entire staff of the Department of Computer Science here at IUPUI who have taught me various computer science related courses, which has extensively helped me in this study.

I am particularly grateful for the assistance and direction given by Dr. Katherine Kula, who always encouraged me at all the stages of this thesis. She is indeed one of the most encouraging persons I have met in a long time. I express my sincere gratitude to Dr. Katherine Kula and Dr. Ahmed A. M. Ghoneima for providing me with their technical data sets for carrying the experiment required for this study.

I would like to offer my sincere thanks to Dr. Dennis L. Rudnick for supporting me and encouraging me throughout my research, supporting me throughout all my hardships and for helping me cope up with the stress. Finally, I wish to thank my family for their constant support and encouragement throughout my study.

TABLE OF CONTENTS

TABLE OF CONTENTS.....	5
LIST OF TABLES.....	7
LIST OF FIGURES	8
ABSTRACT.....	12
1. INTRODUCTION	13
1.1 Motivation.....	13
1.2 Problem Statement	14
1.3 Contributions of this Thesis	15
1.4 Organization of Thesis	16
2. BACKGROUND.....	17
2.1 Previous Work.....	17
2.2 Prior Work on Facial Registration and Reconstruction	17
3. METHODOLOGY	20
3.1 Materials and Data	21
3.2 Data Processing.....	22
3.2.1 Preprocessing and Data Extraction	22
3.2.2 Generating Face Meshes	25
3.2.2.1 Data Preparation	25
3.2.2.2 Skull Surface Extraction (Segmentation)	26
3.2.2.3 Outer Skin Extraction (Segmentation)	29
3.2.2.4 Isosurface Creation.....	31
3.3 Surface Registration.....	33
3.3.1 Rigid Iterative Closest Point (ICP)	33
3.3.2 Optimal Step Non-Rigid Iterative Closest Point (NRICP)	36
3.3.3 Registration Algorithm	40
3.4 Reconstruction of Facial Data.....	40
3.5 Facial Appearance Transition with Physical Variants	46
3.5.1 Evaluating Face Thickness Changes.....	48
3.5.2 Reshaping and Deformation.....	53

3.5.2.1	Skin Depths Evaluation for Reshaping.....	53
3.5.3	Deforming Face Shape.....	55
4.	RESULTS	57
4.1	Facial Reconstruction Results.....	57
4.1.1	Quantitative Analysis.....	57
4.1.2	Qualitative Analysis.....	57
4.1.2.1	Testing	65
4.1.2.2	Validity Testing	65
4.1.2.2.1	Face Validity	65
4.1.2.2.2	Content Validity	65
4.1.2.2.3	Concurrent Validity.....	66
4.1.2.3	Reliability Testing	66
4.1.2.3.1	Test-Retest.....	66
4.1.2.3.2	Alternate Form	69
4.1.2.3.3	Equivalent Form.....	74
4.2	Facial Appearance Change Results.....	80
4.2.1	Illustration 1	80
4.2.2	Illustration 2	82
4.2.3	Illustration 3	84
5.	DISCUSSION.....	86
6.	CONCLUSION.....	88
	REFERENCES	89

LIST OF TABLES

Table 1: TABLE for vertex markers (De Greef et al., 2006).....	49
Table 2: Partial Regression coefficients at the selected landmarks	54
Table 3: Hit rate of each slide in column 2, Choice count and the percentage of hit rate of each slide in column 3, Percentage.	64

LIST OF FIGURES

Figure 2-1 : American method of manual facial reconstruction (Caroline Wilkinson, 2010).....	17
Figure 3-1: Flow chart of experimentation	20
Figure 3-2: Flow chart for data processing	22
Figure 3-3: Valid skin sample (a) frontal view (b) side view	23
Figure 3-4: Samples that are not considered due to missing information. (a) missing supraorbital and eyebrows information (b) missing nose information (c) missing nose information.....	23
Figure 3-5: Head scans of sample who had cleft palate (a) front view (b) side view.....	24
Figure 3-6: Horizontal 250 th slice of a whole head scan (a) original cross-section of the 250 th slice, with 2 extremes on top and bottom being the tip of the nose and the back of the skull (b)front half of the face which includes all the facial features as in eyes, nose, lips, etc.....	26
Figure 3-7: Horizontal 250 th slice, by the tip of the nose, represented at different stages of segmentation and processing. (a) Original 250 th slice without any manipulation (b)Face front extracted from original 250 th slice (b) Segmented skull (c) Skull holes filled filled according to algorithm.	27
Figure 3-8: Horizontal 400 th slice, by the lower jaw, represented at different stages of segmentation and processing. (a) Original 400 th slice without any manipulation (b)Face front extracted from original 400 th slice (c) Segmented skull (d) Skull holes filled according to algorithm.....	28
Figure 3-9: Horizontal 250 th slice, by the tip of the nose, represented at different stages of skin segmentation and processing. (a) Original 250 th slice without any manipulation (b)Face front extracted from original 250 th slice (b) Segmented skin (c) Skin holes filled filled according to algorithm.....	30
Figure 3-10: Horizontal 400 th slice, by the lower jaw, represented at different stages of skin segmentation and processing. (a) Original 400 th slice without any manipulation (b)Face front extracted from original 400 th slice (c) Segmented skin (d) Skin holes filled according to algorithm.....	31

- Figure 3-11: Isosurface generated on a sample patient data, PatientSkin1. (a) Raw face isosurface with 2202684 faces and 1101344 vertices. (b) Raw face isosurface zoomed-in in the highlighted spot. 32
- Figure 3-12: Reduced isosurface generated on a sample patient data, PatientSkin1. (a) Reduced face isosurface with 2000 faces and 1002 vertices. (b) Reduced face isosurface showing the triangulation (faces and vertices). 33
- Figure 3-13: Overlapping the meshes for registration purposes. (a) Source bone mesh of one of the Patient overlapped onto the target bone mesh (PatientBone1). (b) Source skin mesh overlapped onto the target skin mesh (PatientSkin1). 34
- Figure 3-14: Meshes after Rigid ICP. (a) Source and target bone meshes after Rigid ICP (b) Source and target skin meshes after Rigid ICP. 35
- Figure 3-15: Meshes after Non Rigid ICP, completing the registration step. (a) Source and target bone meshes overlapped at the end of registration. (b) Source and target skin meshes overlapped at the end of registration. 37
- Figure 3-16: Original and reconstructed faces of one test data. (top-left) Original face of the test data, frontal view (top-right) Reconstructed face of the test data, frontal view (bottom-left) Original face of the test data, side view (bottom-right) Reconstructed face of the test data, side view. 44
- Figure 3-17: Original and reconstructed faces of one of the test data. (top-left) Original face of the test data, frontal view (top-right) Reconstructed face of the test data, frontal view (bottom-left) Original face of the test data, side view (bottom-right) Reconstructed face of the test data, side view. 45
- Figure 3-18: Interactive interface for observing facial changes depending on age and BMI. 47
- Figure 3-19: Model skull surfaces with vertex makers labelled as 'X' (a) Skull frontal view with vertex markers (b) Skull side view with vertex markers. 50
- Figure 3-20: Bone and corresponding skin vertex marker. (top) Bone and skin mesh overlapped highlighting the bone vertex marker and its corresponding closest skin vertex. (bottom) Highlighted patch from the top image showing bone vertex marker [855] and its closest skin vertex [743] 52
- Figure 3-21: The above figures show the skin vertices (X) corresponding to the bone vertex markers before and after modifying with respect to the increase in BMI to 2.

The figure (a) and figure (b), when observed has marked skin vertex points that are displaced depending on the thickness difference calculated.	55
Figure 4-1: Pie chart showing the number of participants in each age group. The age group considered are given below.	59
Figure 4-2: Slide 1. Top image is the test image which is also the reconstructed image that must be matched with one of the 6 images (2nd and 3rd row face pool). Click on one of the pictures from the face pool selects the respondent's choice.	61
Figure 4-3: Slide 13. Top image in row 1 is the test image that is to be matched to one of the six images in row 2 and 3. The correct answer being the first image from left in row 3. The statistics are shown in the figures below.....	62
Figure 4-4: A breakdown view of the responses report for slide 13. The top pick being the expected image with a hit rate of 58 responses that is picked about 80.56% when compared to other faces in the pool. If observed, the total count of responses is 72 for 5 faces where one face did not get a single response (first face from the left in row 2 in figure) showing majorly chosen face to be the expected answer.	63
Figure 4-5: The bar chart of the choice count of the responses of slide 13 of figure. The most prominent bar being the expected face choice count from the live respondents.....	64
Figure 4-6: Slide 1 repeated as slide 8 in the survey.	67
Figure 4-7: Slide 1 face pool choice count and choice percentages.	68
Figure 4-8: Slide 8 face pool choice count and choice percentages. The other 2 faces had 0 picks and so are not presented in the report.	69
Figure 4-9: Slide 4 from the survey	71
Figure 4-10: Slide 9 from the survey	72
Figure 4-11: Slide 4 Choice count and choice percentage for each face in the pool.....	73
Figure 4-12: Slide 9 Choice count and choice percentage for each face in the pool.....	74
Figure 4-13: Slide 11 from the survey	76
Figure 4-14: Slide 15 from the survey	77
Figure 4-15: Slide 11 Choice count and choice percentage for each face in the pool.....	78
Figure 4-16: Slide 15 Choice count and choice percentage for each face in the pool.....	79

- Figure 4-17: BMI change results on Interactive tool. First image: original face with no BMI and age changes. 2nd image: Slider on the bottom moved to the right (highlighted by an oval shape). New age and BMI are displayed in a message box every time slider is moved. 3rd image: New facial appearance with the changed BMI. 81
- Figure 4-18: Age change results on Interactive tool. First image: original face with no BMI and age changes. 2nd image: Vertical slider on the right has been moved upwards (highlighted by an oval shape). New age and BMI are displayed in a message box every time slider is moved where new age is 77.5 years. 3rd image: New facial appearance with the changed age. 83
- Figure 4-19: Age and BMI change results on Interactive tool. First image: original face with no BMI and age changes. 2nd image: Horizontal slider for BMI is moved to the right changing the BMI to 5.08 and vertical slider on the right has been moved upwards (highlighted by an oval shape) changing the age to 58.5. The new age and BMI are displayed in the message box. 3rd image: New facial appearance with the changed age and BMI is displayed. 85

ABSTRACT

Author: Gorilla, Anusha. MS

Institution: Purdue University

Degree Received: August 2019

Title: Data Driven Dense 3D Facial Reconstruction from 3D Skull Shape.

Major Professor: Mihran Tuceryan

This thesis explores a data driven machine learning based solution for Facial reconstruction from three dimensional (3D) skull shape for recognizing or identifying unknown subjects during forensic investigation. With over 8000 unidentified bodies during the past 3 decades, facial reconstruction of disintegrated bodies in helping with identification has been a critical issue for forensic practitioners. Historically, clay modelling has been used for facial reconstruction that not only requires an expert in the field but also demands a substantial amount of time for modelling, even after acquiring the skull model. Such manual reconstruction typically takes from a month to over 3 months of time and effort. The solution presented in this thesis uses 3D Cone Beam Computed Tomography (CBCT) data collected from many people to build a model of the relationship of facial skin to skull bone over a dense set of locations on the face. It then uses this skin-to-bone relationship model learned from the data to reconstruct the predicted face model from a skull shape of an unknown subject. The thesis also extends the algorithm in a way that could help modify the reconstructed face model interactively to account for the effects of age or weight. This uses the predicted face model as a starting point and creates different hypotheses of the facial appearances for different physical attributes. Attributes like age and body mass index (BMI) are used to show the physical facial appearance changes with the help of a tool we constructed. This could improve the identification process. The thesis also presents a methods designed for testing and validating the facial reconstruction algorithm.

1. INTRODUCTION

This thesis involves building a predicted 3D shape of a face by reconstructing the skin from the 3D skull shape that can be used for forensic identification purposes. This is a novel method for Cranio-Facial Reconstruction and Identification because in addition to the prediction of approximate 3D facial shape from the 3D skull shape it also includes modeling factors like age and weight as represented by body mass index (BMI) value. This allows an expert to generate possible facial shape predictions interactively making the task of successful recognition more probable.

1.1 Motivation

There have been many technological developments in the past two decades. With the increase in technology and advancement, many areas of forensic science tried to improve their functionality by incorporating contemporary techniques into solving practical problems. An example is Missing Person and Unidentified Person cases in which the usual data for identification is not available except for skeletal remains found. The Federal Bureau of Investigation's National Crime Information Center (NCIC) is reported with thousands of Missing Person cases per year. The active cases of NCIC by the end of December, 2018, was around 85,459. Almost 8,135 unidentified person records have been reported since 1983 and approximately 1300 were canceled by the end of December, 2018, due to being invalid or being identified (National Crime Information Center's (NCIC's), 2018). Although DNA analysis has been helpful in identifying many of these cases, the fact that so many thousands of cases are still unidentified suggests that additional methods of identification are necessary.

Often, in a crime scene there could be human corpses which are to be identified to proceed with further investigation. In cases when a partially damaged body is found, the investigators use existing forensic methods to identify the individual. These methods include identifying the DNA samples of the body, dental identification, identifying fingerprints, etc. But this identification becomes extremely difficult when the cadaver is decomposed, skeletonized or mutilated. This is when the bone structure could be used as a basis for identification as it is less affected by the external conditions. One way of identifying the body is to build a predicted face using the skull

structure, if the skull is not mutilated, damaged, or destroyed. This method of constructing the face using unidentified skull is known as Cranio-Facial Reconstruction (C. Wilkinson et al., 2006).

In recent years, different reconstruction techniques have been developed to help in the identification process. Studies are based on data from different racial populations and different criteria are used for finding a certain race's soft tissue thickness on the face that could be used for facial reconstruction (Tedeschi-Oliveira, Melani, de Almeida, & de Paiva, 2009). Despite the extensive increase in efforts, there have been shortcomings when it came to diverse data collection, testing and showing efficient results (Bon-Woo & Seong-Whan, 2003). The results can differ depending on what type of data is used (MRI, CT or CBCT), number of data samples, methods used, etc. There is a definite possibility of improvement in the current methodologies as most of them do not consider the multivariate nature of human features but simply use the univariate features like tissue depths and regression equations.

1.2 Problem Statement

The purpose of this study is to build an automated and interactive tool which can help in the reconstruction of 3D face shape from the skull shape. This study also presents a graphical user interface (GUI) for viewing the changes in the facial appearance with change in physical variants like age and weight as represented by body mass index (BMI). Primarily called the cranio-facial reconstruction, the process is used to generate an approximate shape of the face using the outer surface of the skull and soft tissue thickness layered over the skull. The approach is a data driven approach in which a collection of 3D Cone Beam CT (CBCT) scan images are used to learn the tissue thickness over the skull in a given population of humans. The underlying assumption is that the tissue thickness across the face follows the same trends across different people and the variation in the face shapes are, to a first approximation, due to the underlying shape of the skull's bone shape. Machine learning techniques are used for determining the facial soft and hard tissue relationships, predicting the facial form from the data collected. The goal of this method is to generate a predicted facial shape that is closest to the actual facial shape using the available information that could help in recognizing the unidentified body. This generation process might sometimes lead to positive identification, but many times the age or the BMI of the face generated could be different from the face familiar and identifiable and this could lead to a lack of identification. To overcome this disadvantage, this study also presents a method by which after the

predicted face is reconstructed over the skull shape, it is then interactively deformed to predict the face shape for different ages and/or BMI values giving the examiner a tool for generating various hypotheses. To assess the precision and accuracy of the reconstruction, we created a resemblance rating or a survey with a pool of faces by choosing the closest matched face with the reconstructed face.

1.3 Contributions of this Thesis

This thesis presents an approach to predicting the 3D face shape of an unidentified body with the aim of recognizing or identifying the unknown subject. The approach involves considering three-dimensional cone-beam computed tomography (3D CBCT) data of healthy subjects' heads as the basis of learning the relationship of soft tissue thickness relative to bone on various locations on the skull. The contributions are listed below:

- **Predicting a face model**

The dense mesh representation of tissue thickness data by fitting a 3D mesh model of bone and skin to the 3D CBCT data was developed. By using the same mesh model that is fit to the data, the correspondence of the same point on the bone and skin is established by default, thus giving us the tissue thickness at that point. The mesh resolution can be adjusted, resulting in less or more dense data.

- **Machine learning for predicting the face shape**

A method was developed to learn the dense tissue thickness using the bone and skin meshes applied to the CBCT data.

- **Validation using qualitative analysis**

A method was developed to assess whether and how well the reconstructed face was helpful in recognizing the subject. A live survey is conducted where participants are asked to match the algorithmically generated face against a pool of face images, one of them being the correct original match. Mimicking the Forensics' missing person identification, this step is used in validating and assessing the reliability of the algorithm.

- **Facial Appearance Changed at different BMI and age**

Modeling the effects of age and weight on the appearance of the 3D face shape was developed. A tool was also developed that allowed an examiner to interactively change the appearance according to these parameters. This interface can be used by anyone without the knowledge of coding and software.

1.4 Organization of Thesis

The remainder of this thesis is organized as follows. Chapter 2 gives the background and literature survey of related work. Chapter 3 describes the methodology used in predicting the facial reconstruction from a skull. Chapter 4 presents the results. Chapter 5 discusses the results, and finally Chapter 6 gives some conclusions.

2. BACKGROUND

2.1 Previous Work

The state of the art in facial reconstruction has been manual reconstruction by an expert using different techniques like sculpting muscles over the skull with clay and later sculpting skin onto the whole model called Russian method; or using thickness dowels or pegs that are placed at many points on the skull which represent the soft tissue thicknesses over the face at predetermined points and then sculpting the face using these dowels [American]; or using both methods together [Manchester] as mentioned in (Shrimpton et al., 2014). The main disadvantages of the 3D manual reconstruction are (i) the large amount of time to reconstruct the face; (ii) the dependence on subjective interpretation of the expert doing the sculpting; and (iii) the variability of the reconstructed faces among experts doing the reconstruction. Often it takes somewhere between a month to around 3 months to sculpt and reconstruct a face depending on the expertise of the artist. To overcome this disadvantage, the development of computer technology has been used for Facial reconstruction, known as Computer Aided Cranio-Facial Reconstruction, where computerized techniques and algorithms have been used to generate face and to make the generation process quick and smooth.



Figure 2-1 : American method of manual facial reconstruction (Caroline Wilkinson, 2010).

2.2 Prior Work on Facial Registration and Reconstruction

Facial reconstruction using computer-based methods has evolved over time. The most commonly used methods and the evolution is explained in (De Greef & Willems, 2005). Starting

from capturing the skull data, Manhein et al. (Manhein et al., 2000) is the first to use ultrasound to get the soft tissue and bone structure visuals which were used to find the soft tissue thickness data. This was replaced by the usage of CT and MRI scanning techniques to get the bone and soft tissue data for building 2D facial reconstruction as in (Phillips & Smuts, 1996) and (Vignal & Schuliar, 2002). Later, 3D CT volume data was used for the precise soft tissue depth data. Another usage of the CT volume data is to study new techniques to predict the facial soft tissue features. Once the volume data is successfully gathered, then registration (Subsol & Quatrehomme, 2005) of 3D shapes is used for capturing the skull and skin shapes, by creating a generic model and fitting and deforming it to the newly found samples. The 3D model mask generated by registration is used to map the 3D skull structure of new data by scaling and warping the model onto the 3D skull structure. Statistical methods are later used for reconstruction.

(Blanz & Vetter, 1999) presented two different ways for image registration or mapping for postmortem identification. In the first approach, Thin Plate Splines (TPS), a non-rigid registration method that helps warping a reference template onto unidentified skull was used. The second method creates a template of the skull using automatic segmentation that can then be mapped or morphed onto new skull samples and registers the test samples simultaneously. (Berar, Desvignes, Bailly, & Payan, 2005) and (Tu et al., 2005) presented different techniques for facial reconstruction in which both use marching cubes algorithm for skin and skull extraction from computer tomography data and statistical methods are then used for reconstruction. (Tu et al., 2005) uses alignment points for rigid and non-rigid deformations to register the skull and face and the projected models are converted into 2D data with depth intensities in a cylindrical coordinate system that is further used for statistical reconstruction. (Berar et al., 2005), on the other hand, uses a symmetric matching algorithm to register the 3D meshes which are later projected into 2D space and used for reconstruction using statistical methods. (Bon-Woo & Seong-Whan, 2003) proposed a framework for reconstruction of partially damaged faces using a morphable face model. This framework particularly uses 2D images where the shape and texture information are used to estimate the shape and texture of the partially deformed face with the help of Least Squares Minimization. Forward and backward warping are used to reconstruct the new face with estimated shape and texture. (Claes, Vandermeulen, De Greef, Willems, & Suetens, 2006) presented a framework of deformable face models for Cranio-Facial reconstruction which uses TPS-PCA-based Model Fitting which is a combination of statistical method, Principal component analysis

(PCA) and Thin Plate Spline (TPS) procedure. The fitting of the model is done using a few skull landmark points and TPS's minimal bending and then applied to face specific statistical model parameters. The main difference between the existing methods and our method is that all the data generated is in 3D format and all the operations are done on the 3D data, preserving the data and the importance of the facial structure and also the registration undergone, matches the skull and skin models as close as possible to improve and provide accurate results for the reconstruction.

In our method, we try to capture as much variation as possible from the skull and the face by matching the skulls closely to the generic templates using local deformations and global deformations multiple times. Another difference is that our method also models other facial properties like BMI and age effects after the reconstructing the unknown face is done.

Once the best registration is captured, statistical and machine learning methods are used for the reconstruction of the face. In most methods, this reconstructed face is used for recognition purposes but the main disadvantage of using the reconstructed face directly could be that the face generated might be familiar when the person was a particular age or when the person was overweight or when the person was thin and these changes cannot be incorporated to generating a face appearing a little old or young or appearing a little fat or thin. This aspect brings into context a whole variety of identifications and not appearing at a certain age or weight might lead to wrong identification. (Claes et al., 2006) proposed a framework which includes the age, BMI and gender to generate a property-dependent reconstruction of the face using statistical methods but this method is not interactive and has to be executed every time there is a change in the age or BMI or gender.

3. METHODOLOGY

In this section we describe our approach to predicting the 3D face shape from the skull geometry using collected 3D CBCT data. In addition, we also describe our modeling of the effects of weight (parameterized by BMI) and of age on the face shape. The aim is to be able to generate many possible predicted faces that may result in the successful identification of the unknown subject from the facial shape.

The overall approach relies on a collection of 3D CBCT data from which the relationship of bone to skin tissue thickness is learned over a dense set of points over the face. This learned knowledge is then used to reconstruct the predicted face from the 3D skull shape of an unknown subject. The method is divided into 4 stages which is demonstrated using the flow chart in Figure 3-1. These 4 stages are explained in detail in the sections below.

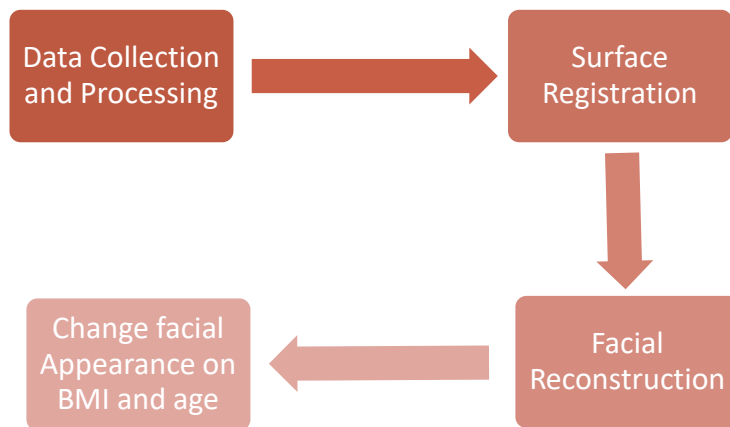


Figure 3-1: Flow chart of experimentation

All the CBCT data obtained are from a single machine thus making the data in the set comparable. For extracting the skull and face surfaces from the head scans, a simple segmentation method is used to identify points in the volume data that represent the bone surface of the skull and the skin surface. This process is repeated over all the CBCT scans and the skull and face surfaces of all the subjects are extracted.

Following the extraction of bone and skin surfaces from the volume data, these surfaces are converted to a 3D mesh model. This is accomplished by using a generic mesh model which is

deformed to fit the extracted surfaces from the data. The same 3D mesh model is used for both skin and bone surfaces. Using the vertices in these two fitted mesh models, we also get the point correspondences by default in the two surfaces. Once the fitted meshes are generated, this data is treated as an extremely high dimensional vector and statistical and machine learning methods and Principal Components Analysis (PCA) is used to represent the valid skull and skin face subspace (Berar et al., 2005). This computed subspace which is computed from the training data is then used to predict the face shape of an unknown subject by obtaining the skull mesh for it and using it to obtain the missing skin vertices using least squares fitting. Finally, the effects of age and weight are modeled by deforming the basic predicted face shape via the above process through an interactive user interface.

Once the faces are reconstructed using the techniques mentioned, the efficacy and accuracy of the system is evaluated using a survey with respondent of all age groups. The results from this survey are further used for reliability and validity of the system.

3.1 Materials and Data

For this framework, we considered a collection of anonymized 3D Cone Beam Computed Tomography (CBCT) volume images as our database upon which the facial reconstruction is based. Our project has been approved by the Institutional Review Board (IRB). The CBCT data is obtained with i-CAT CBCT (Imaging Sciences, Hatfield, PA) set for full 13 cm field of view, 20 sec of scanning time, and a resolution of 0.4 mm voxel size of the School of Dentistry, Indiana University. Consent was received from a total of 70 patients to undergo a 3D CBCT scan to capture their head data. The number of males and females are 55 and 15, respectively. The age range of males is 18-35 and the age range of females is 19-27. The scans of the head are stored in a DICOM format whose size is 768 X 768 X 576. Each sample's file consisted of the head scan from the top of the eyebrows i.e., from the supraorbital line until the upper neck part, i.e., beneath the chin. With the head scans, we also gathered the patients' characteristic attributes, such as Code, Last Name, First Name, Patient #/CBCT #, Gender, Ethnicity, Age (Years), Age (Months), Total Age (months) to distinguish the patients during results. All this information was first consented and then gathered. Due to a smaller number of female scans, we were only able to consider the male head scans for reconstruction, and we were unable to include female patients' scans in the reconstruction. All the scans used for this project

are Caucasian males. The whole framework was run on a Windows 7 Enterprise OS including a 4 core Intel Core i5 processor with 8 GB RAM using Matlab R2016a.

3.2 Data Processing

The data processing step involves data collection and processing whose flow is as follows:

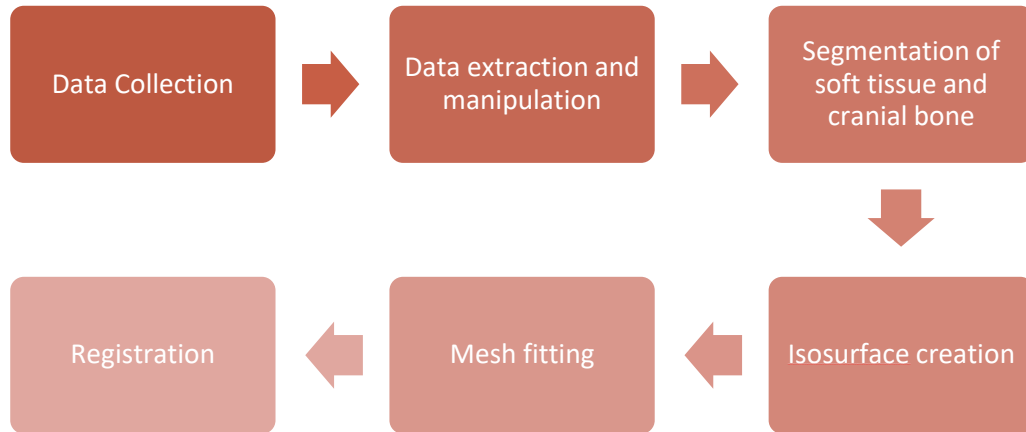


Figure 3-2: Flow chart for data processing

3.2.1 Preprocessing and Data Extraction

The CBCT scans obtained were inconsistent with each other in terms of the region of the head scanned. Many of the scans were obtained from the eyebrows downward, missing the forehead or supraorbital information. Many other scans had been taken up to the chin and not beneath the chin. In order to have our data comparable and consistent, we considered the head scans starting from just below the supraorbital line, between the eyebrows and supraorbital line to the chin line, shown in **Error! Reference source not found.**, for reconstruction.

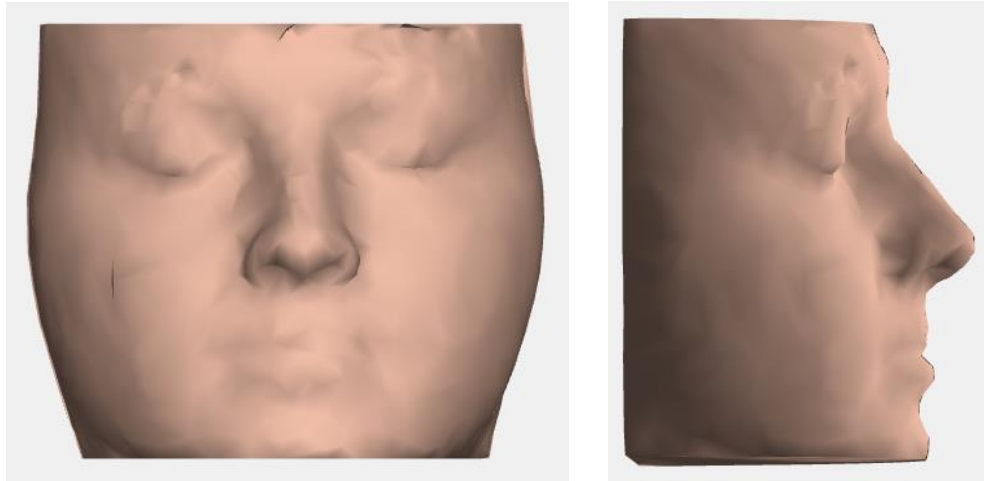


Figure 3-3: Valid skin sample (a) frontal view (b) side view

The data between these limits is complete and consistent. An example is shown in Figure 3-3, where the eyes, most of the nose structures, cheeks and mouth including the teeth structure were fully present. The missing information had some effect on our facial appearance computation, which we will be discussing in the results section, as the information on the forehead plays an important role in computing the face shape with different BMIs (Zhao, Jin, Huang, Chai, & Zhou, 2018). In the 55 male patient head scans, we were only able to consider 48 samples as 2 males were way out of the age range and 5 male scans had some missing information (e.g., the tip of the nose to a quarter of the nose was missing as shown in the Figure 3-4).

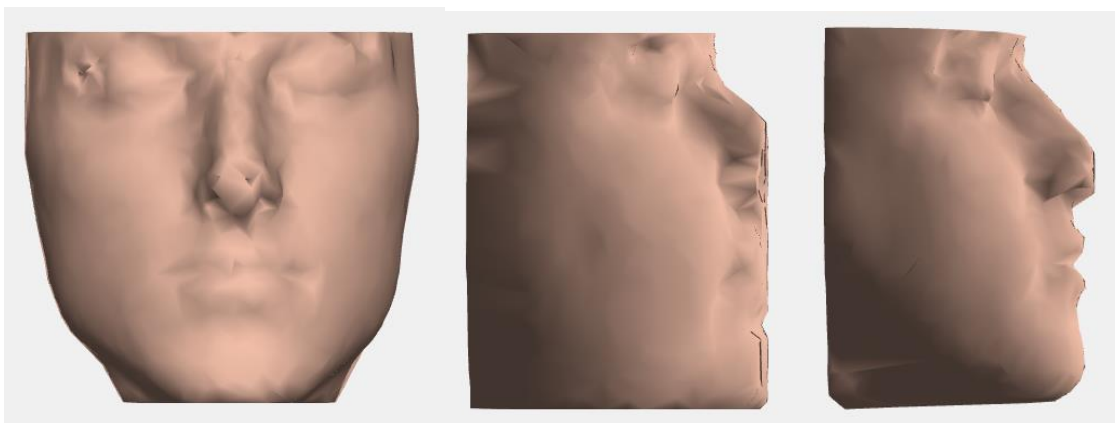


Figure 3-4: Samples that are not considered due to missing information. (a) missing supraorbital and eyebrows information (b) missing nose information (c) missing nose information.

This missing data is due to the CBCT scan and is not due to the algorithm. In the male head scans that were considered for the reconstruction, there were 4 head scans that had a 0.3 mm to 0.6 mm of the tip of the nose trimmed off but we had to consider these scans due to the immense reduction in the number of training data otherwise. Also 3 patient scans out of 48 scans considered, had a surgically repaired cleft lip and palate, as shown in Figure 3-5, which were used in training and reconstruction as decrease in the training data could cause problems with overfitting.

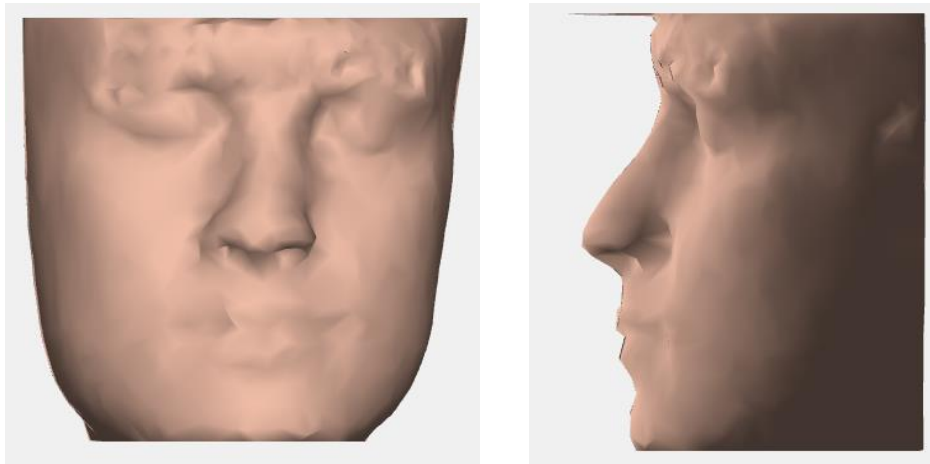


Figure 3-5: Head scans of sample who had cleft palate (a) front view (b) side view.

In this thesis, one patient CBCT scan is left to be a common sample for isosurface mapping. In the remaining 45 sample scans, 35 CBCT scans are used as training data and the remaining 10 sample CBCT scans are used as testing data.

All 48 scan data are first converted into a workable format as follows. The pixel intensities are used to extract the relevant information from the volume data. Firstly, each patient sample is considered, and the bone or skull data is extracted. For this, all the pixels with an intensity below 1300 are marked 0 and the ones above 1300 are considered to form the skull surface. For the skin surface, all the pixels above the intensity 400 are considered and once both the soft tissue and skull tissue surfaces are identified, the inside regions for each are filled as they have no bearing to the external surface shapes. After this, isosurfaces are identified for both the skull and skin. Then a registration method is performed.

3.2.2 Generating Face Meshes

A generic mesh model is used for representing the bone and skin 3D shape information in the sample volumes. This generic mesh model is extracted from one of the volume data samples by identifying the bone and skin isosurface and using the marching cubes algorithm to generate the triangular mesh. This extracted mesh is then used as the generic mesh which is fitted to the other meshes by rigid alignment followed by a deformable registration. The registration process starts with global alignment using rigid iterative closest points (ICP) where the two meshes features are aligned such that they are overlapping each other and make rigid transformations to map one surface onto another globally on whole. Once the two surfaces are rigidly aligned, local transformations are made so that the surface that is mapped is close to the target. The local transformations are done using Optimal Step Nonrigid ICP (Amberg, Romdhani, & Vetter, 2007) where a stiffness measure is considered using which the source surface maps itself closely to the target surface along the normal of the source mesh. The registration process starts with assigning each vertex on the source surface to the closest point on the target surface by nearest-point search. In an iterative loop, the optimal deformations and stiffness are calculated for the source mesh vertices and the new coordinates are found which are used again with new deformation and stiffness until the two meshes converge to a closest epsilon value. The deformation on the mesh are applied more locally with the changes in the values of stiffness, denoting strongly regularized deformations make global deformations with large values of stiffness and the smaller values allow more localized deformations. For each iteration, the stiffness values are decreased to acquire more local deformations, mapping the source close to the target. Using this technique, all the common source isosurface is mapped onto all the other isosurfaces and the final coordinates are obtained, ultimately registering the isosurfaces.

These process described above is discussed in details in different steps in the later sections.

3.2.2.1 Data Preparation

In each of the patient head CBCT scan folder, there are 576 number of images pertaining to the horizontal slices of the head as shown in Figure 3-6. Our goal is to reconstruct the face and examine the appearance changes in the face with age and BMI. For this, the data we need is the front half of the face from the supraglenoid ie., the front of the ear without including the ears. For this, we considered a middle slice from the head scan, which is the 250th slice which would

approximately be a slice of the nose. In this slice, we calculate the two extreme points in the y-axis, which is the tip of the nose and the back of the skull from that horizon. We calculate the number of pixels in the y-axis between these extreme points and divide the number of pixels by 2.2 to get the approximate center of the skull. To consider the first half of the face, this center point is considered as a limit in all the slices and all the pixels in the y-axis that come after the center point are equaled to zero. With this, the front half of the face is extracted from each scan. As the head scans are not consistent with the height of the head, ie., from the supraorbital line to beneath the chin, we first try to control the data and keep it consistent. For this, we consider the slices between the 40th and 500th slices, to have consistent data from beneath the supraorbital line to the chin.

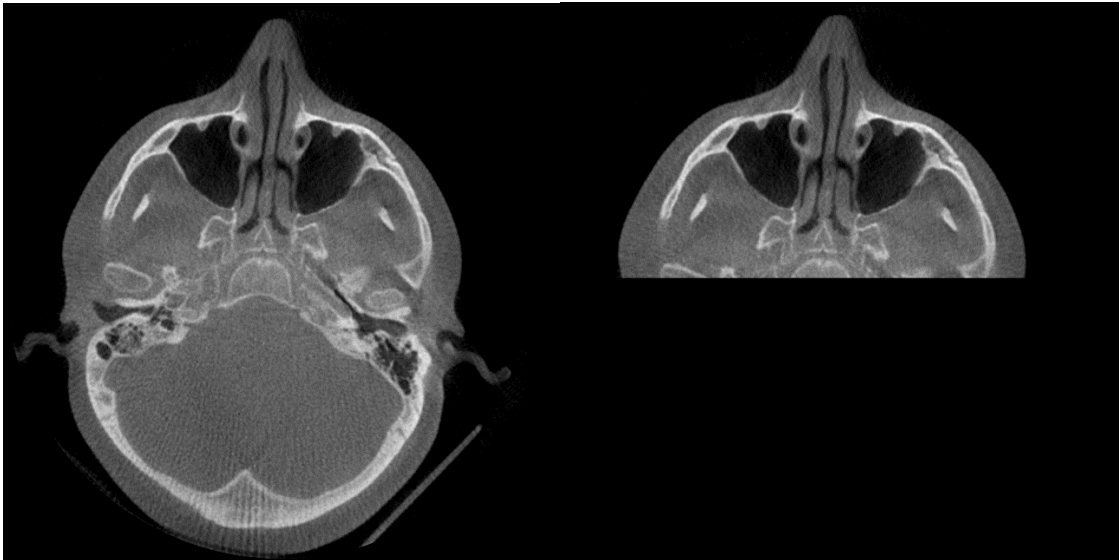


Figure 3-6: Horizontal 250th slice of a whole head scan (a) original cross-section of the 250th slice, with 2 extremes on top and bottom being the tip of the nose and the back of the skull (b) front half of the face which includes all the facial features as in eyes, nose, lips, etc.

3.2.2.2 Skull Surface Extraction (Segmentation)

The extraction of the skull and skin are done differently using isosurface identification, because in this particular application we are interested only in the external surface of the skull and not the interior surfaces. The bone surface and the skin on the head have different intensities in the CBCT data. Extracting the isosurfaces for the bone and skin at the corresponding intensity isosurfaces results in the extraction of the geometry of these two structures. All our scans are obtained from the same machine resulting in the pixel intensities over different scans to be comparable. Therefore, to capture the skull from all the slices around all the scans, we set a

threshold intensity of 1300 and all the pixels above this intensity are considered. With this, the interior and the exterior of the skull is extracted as in Figure 3-7.

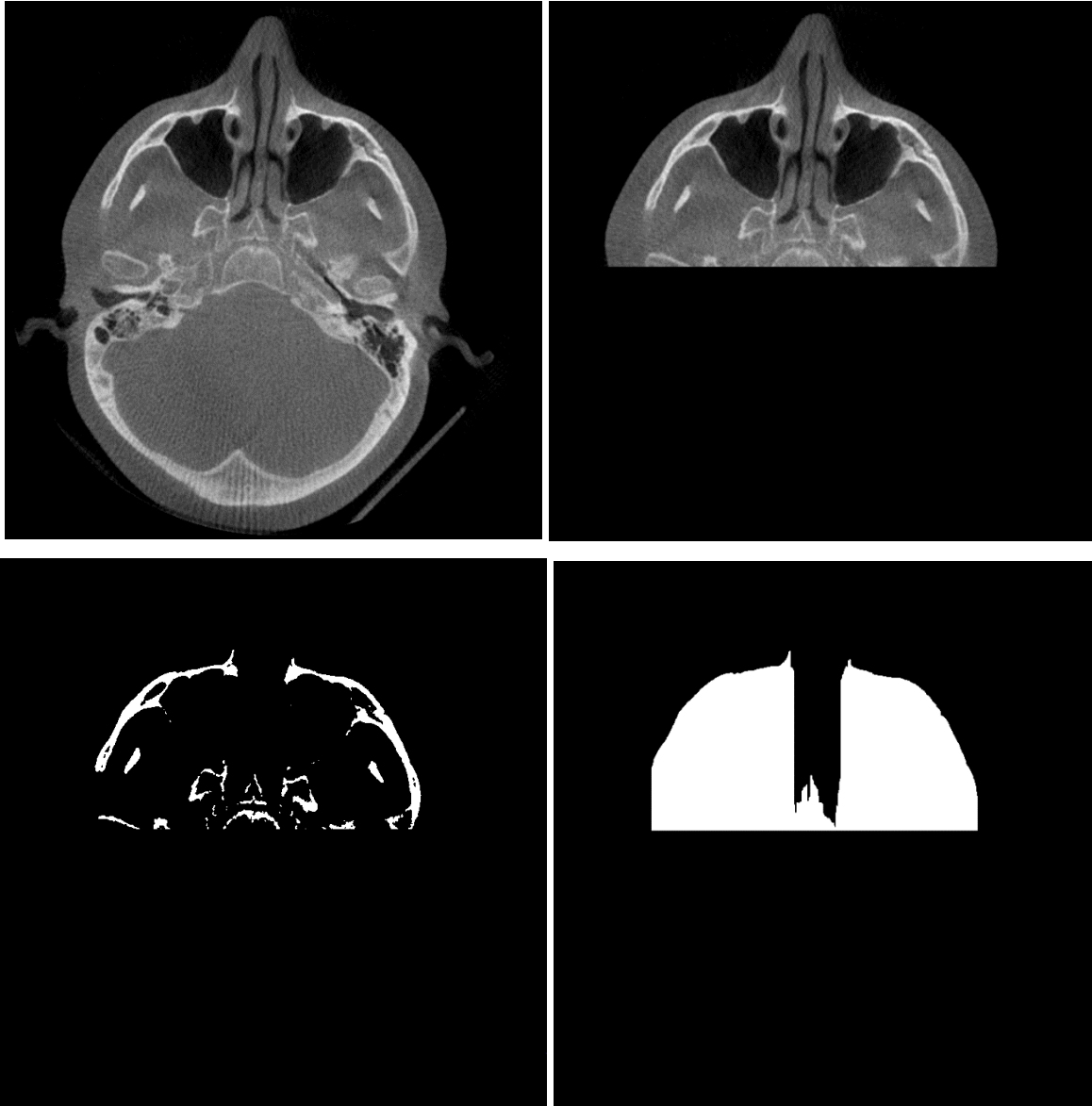


Figure 3-7: Horizontal 250th slice, by the tip of the nose, represented at different stages of segmentation and processing. (a) Original 250th slice without any manipulation (b) Face front extracted from original 250th slice (c) Segmented skull (d) Skull holes filled filled according to algorithm.

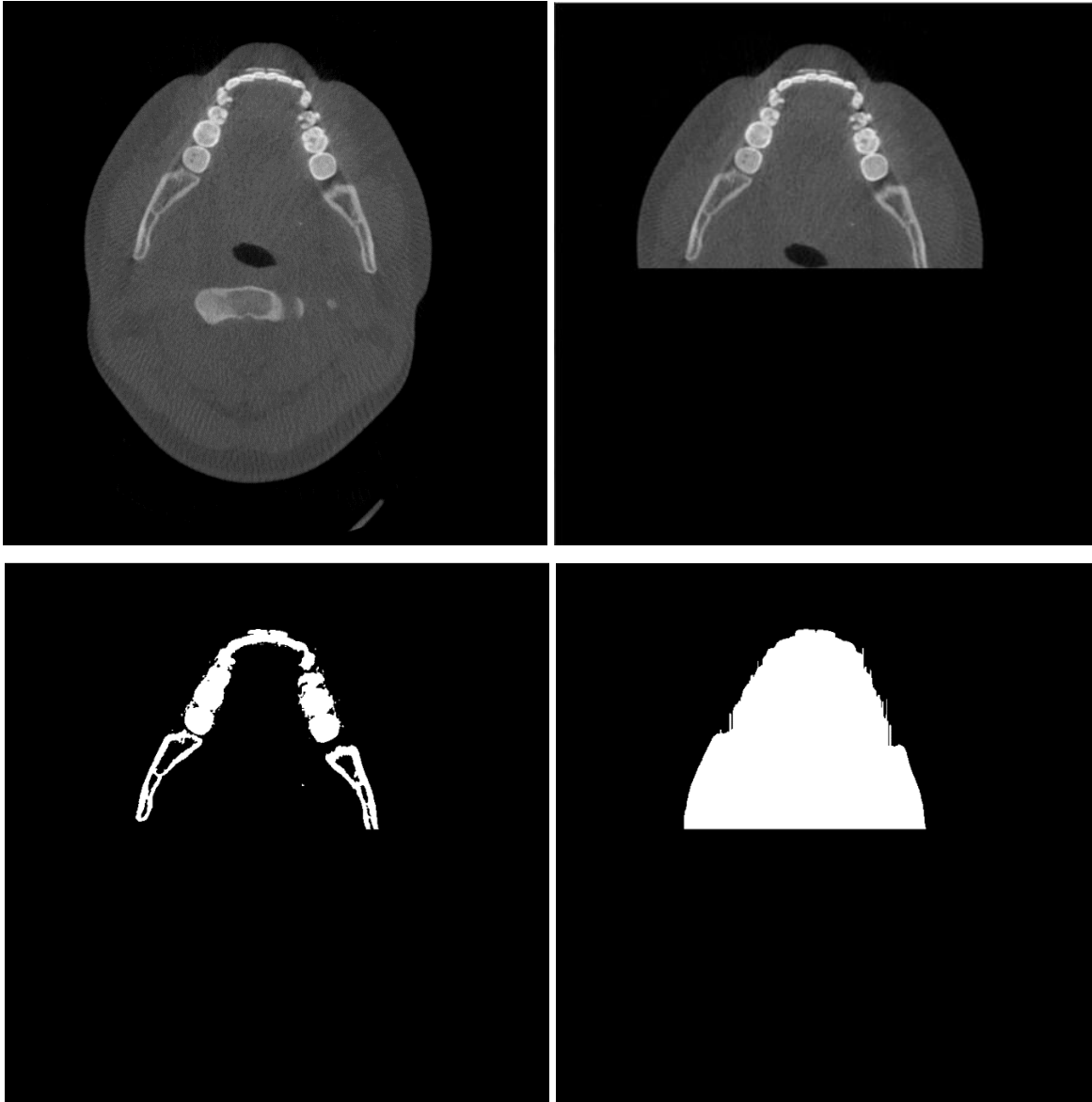


Figure 3-8: Horizontal 400th slice, by the lower jaw, represented at different stages of segmentation and processing. (a) Original 400th slice without any manipulation (b)Face front extracted from original 400th slice (c) Segmented skull (d) Skull holes filled according to algorithm.

Using all this information for creating an isosurface could complicate the process of reconstruction as the algorithm requires the shape of the skull and not the inner parts of the skull. For this reason, the extracted skull shape is filled to eliminate the internal structures such as nasal passages, etc from consideration resulting only in the outer bone surface of the skull. To fill the skull, each slice is considered and the first x-axis pixel encountered in the y-axis, going downwards

is considered and the pixels between that point and y-axis center of the skull are filled, as shown in Figure 3-7 and Figure 3-8. This process is continued for all the x-axes in all the slices. Once all the slices are filled, we have a solid skull model with holes at the optic canal, nasal concha and the extremes of the teeth.

3.2.2.3 Outer Skin Extraction (Segmentation)

After the data processing step, similar to the skull extraction technique, we use the pixel intensity variation for extracting the soft tissue from the scans. Unlike skull data, the soft tissue pixel intensity value is smaller and if the threshold frequency is not set properly extra pixels may be included or they may be lost due to noise. In our CBCT data, the intensity of the background pixels and the noisy pixels are less 350 and all the pixels above 400 represent the soft tissue.

For skin extraction, our goal is to capture the outer appearance of the face and compared to the bone/skull data, extracting the skin surface is more straightforward. Just like the skull, all the pixels with intensity above 400 are extracted. All the extracted pixels whose intensity is above 400 are converted to 400 and all the pixels with intensity less than 400 are changed to intensity - 1000. Once the face is discovered in all the slices, there are many inner details and holes in the slices which are not required and these could interfere with the reconstruction later. For this, the slices are filled so that there are no holes in a process similar to the extraction of the skull. To fill the holes each slice's first x-coordinate pixel in every y-axis that is 400 is taken and all the slices between the x-coordinate pixel and the center of the skull horizontal layer are filled with pixel intensities of 400. Doing this through all the y-axes for all the slices would fill the slices of the face resulting in no holes, as shown in the Figure 3-9 and Figure 3-10.

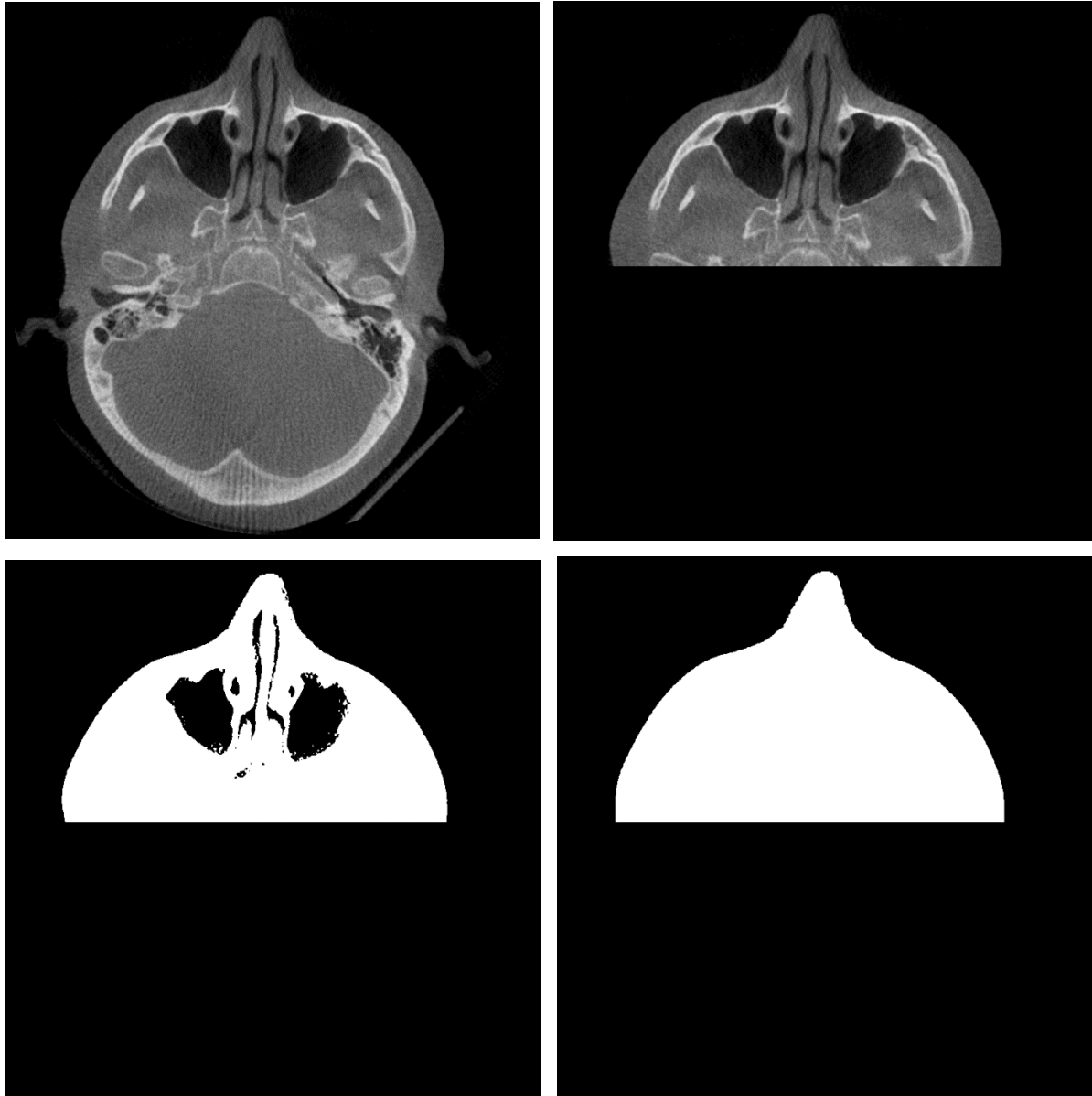


Figure 3-9: Horizontal 250th slice, by the tip of the nose, represented at different stages of skin segmentation and processing. (a) Original 250th slice without any manipulation (b) Face front extracted from original 250th slice (b) Segmented skin (c) Skin holes filled filled according to algorithm.

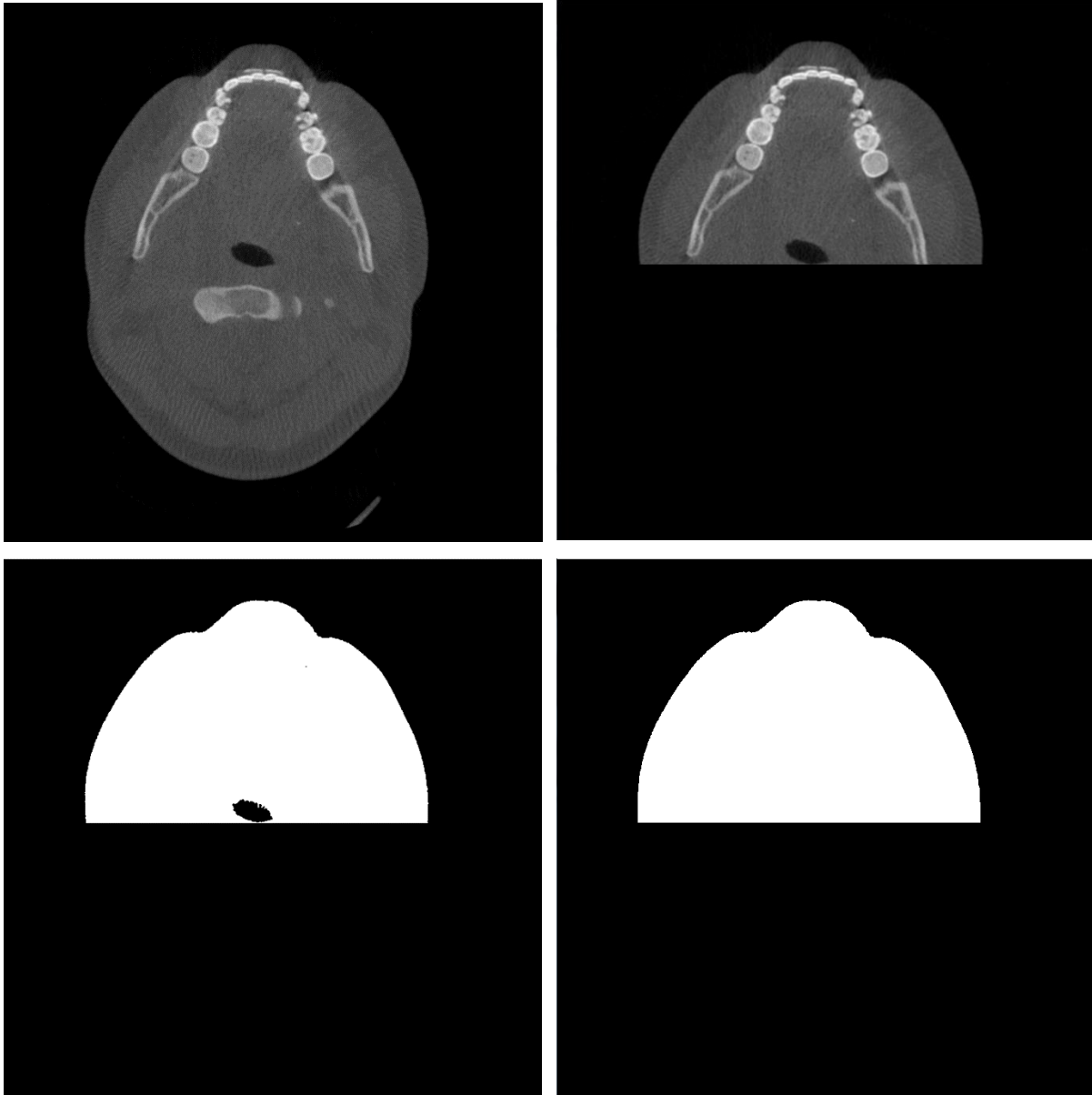


Figure 3-10: Horizontal 400th slice, by the lower jaw, represented at different stages of skin segmentation and processing. (a) Original 400th slice without any manipulation (b) Face front extracted from original 400th slice (c) Segmented skin (d) Skin holes filled according to algorithm

3.2.2.4 Isosurface Creation

Once the skull and face are extracted from the slices, a mesh or a 3D surface is formed from extracted data. The filled skull and face are converted into an isosurface using Matlab's isosurface function. The isosurface function returns a structure array with the triangulation data consisting vertices and faces of the outer skull and skin surfaces. This surface data obtained from

isosurface is very large with 2202684 faces and 1101344 vertices, as shown in the Figure 3-11 and Figure 3-12. This amount of data would need a lot of memory and processing and would consume a lot of time for processing and to avoid this problem we reduce the surface to 2000 faces. This is done using the `reducepatch` (MathWorks Isosurface, 2016) method of Matlab. With the faces and vertices, the vertex normal are also calculated and included into the structure array for further processing and all this structure array is saved in a mat format as “PatientBone” or “PatientSkin” followed by the number assigned to each patient. This process is carried on for the extraction of skull and skin around all the scans.

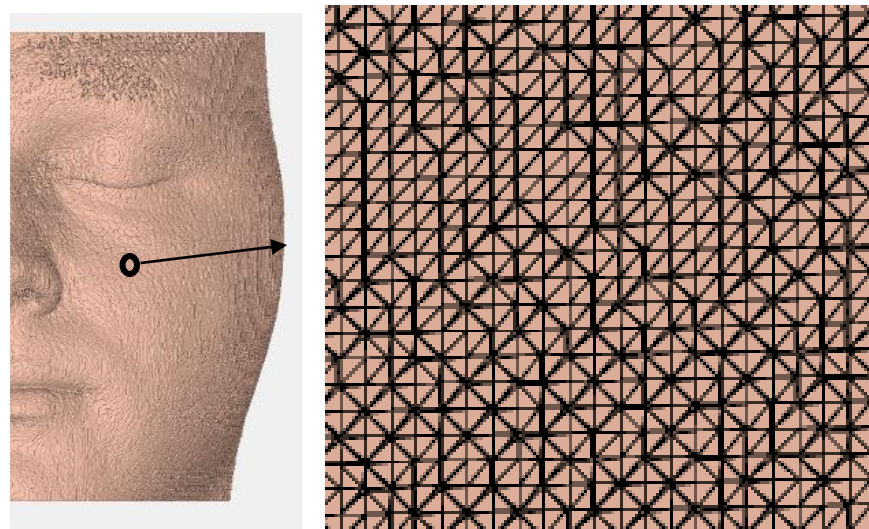


Figure 3-11: Isosurface generated on a sample patient data, PatientSkin1. (a) Raw face isosurface with 2202684 faces and 1101344 vertices. (b) Raw face isosurface zoomed-in in the highlighted spot.

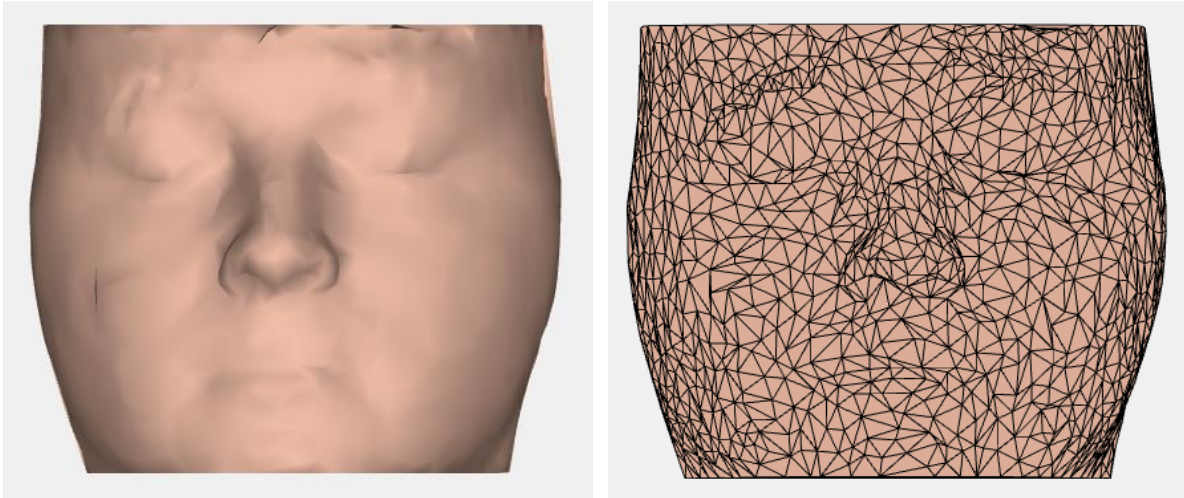


Figure 3-12: Reduced isosurface generated on a sample patient data, PatientSkin1. (a) Reduced face isosurface with 2000 faces and 1002 vertices. (b) Reduced face isosurface showing the triangulation (faces and vertices).

3.3 Surface Registration

Once all the scans are converted into skull and skin meshes, they need to be represented in a uniform parameterization to continue with the reconstruction. The word uniform parameterization signifies that all the data obtained needs to be in one coordinate system. This is done by registration where one surface is mapped or warped onto another surface to take its shape and deformations by forcing some constraints on the algorithm. In this thesis, the Rigid (ICP) (Besl & McKay, 1992) and Non Rigid ICP (NRICP) Algorithms (Amberg et al., 2007) are used for registration of the surfaces. To begin with the implementation, the algorithm starts by considering one template mesh to fit or deform to other meshes. All the created meshes or isosurfaces are inspected closely and “Patient1” skull and face meshes are used as a template to map to the other skull and skin meshes.

3.3.1 Rigid Iterative Closest Point (ICP)

Before the NRICP, the Rigid Iterative Closest Point (ICP) is performed which optimally aligns the template mesh with the target mesh by transforming and scaling the template mesh close to the target mesh, as shown in Figure 3-13 **Error! Reference source not found.** If the meshes are in a different coordinate system, are reversed or are wide apart, the Rigid ICP positions both the meshes on the same plane and scales the template mesh close to the target mesh.

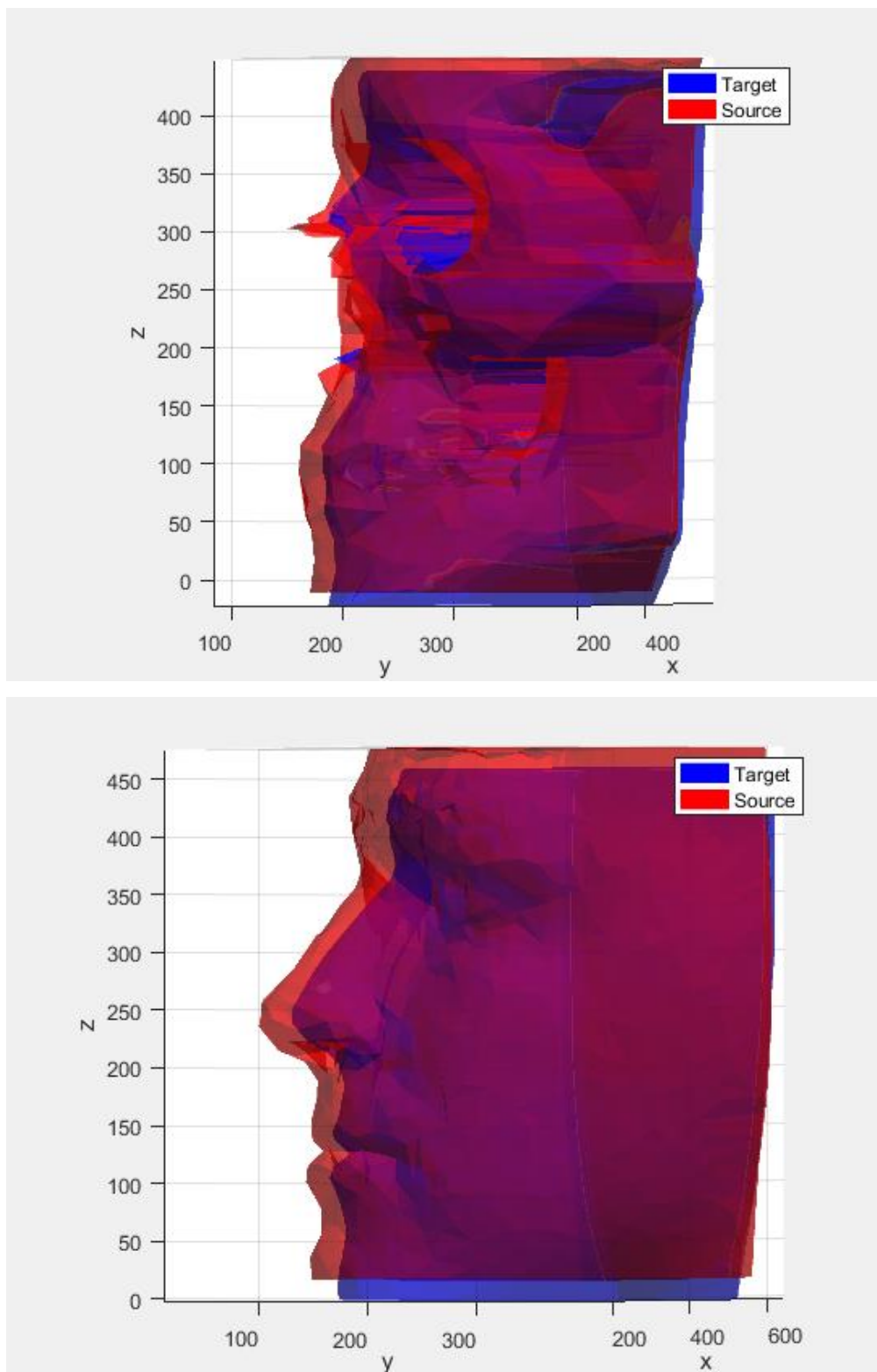


Figure 3-13: Overlapping the meshes for registration purposes. (a)Source bone mesh of one of the Patient overlapped onto the target bone mesh (PatientBone1). (b)Source skin mesh overlapped onto the target skin mesh (PatientSkin1).

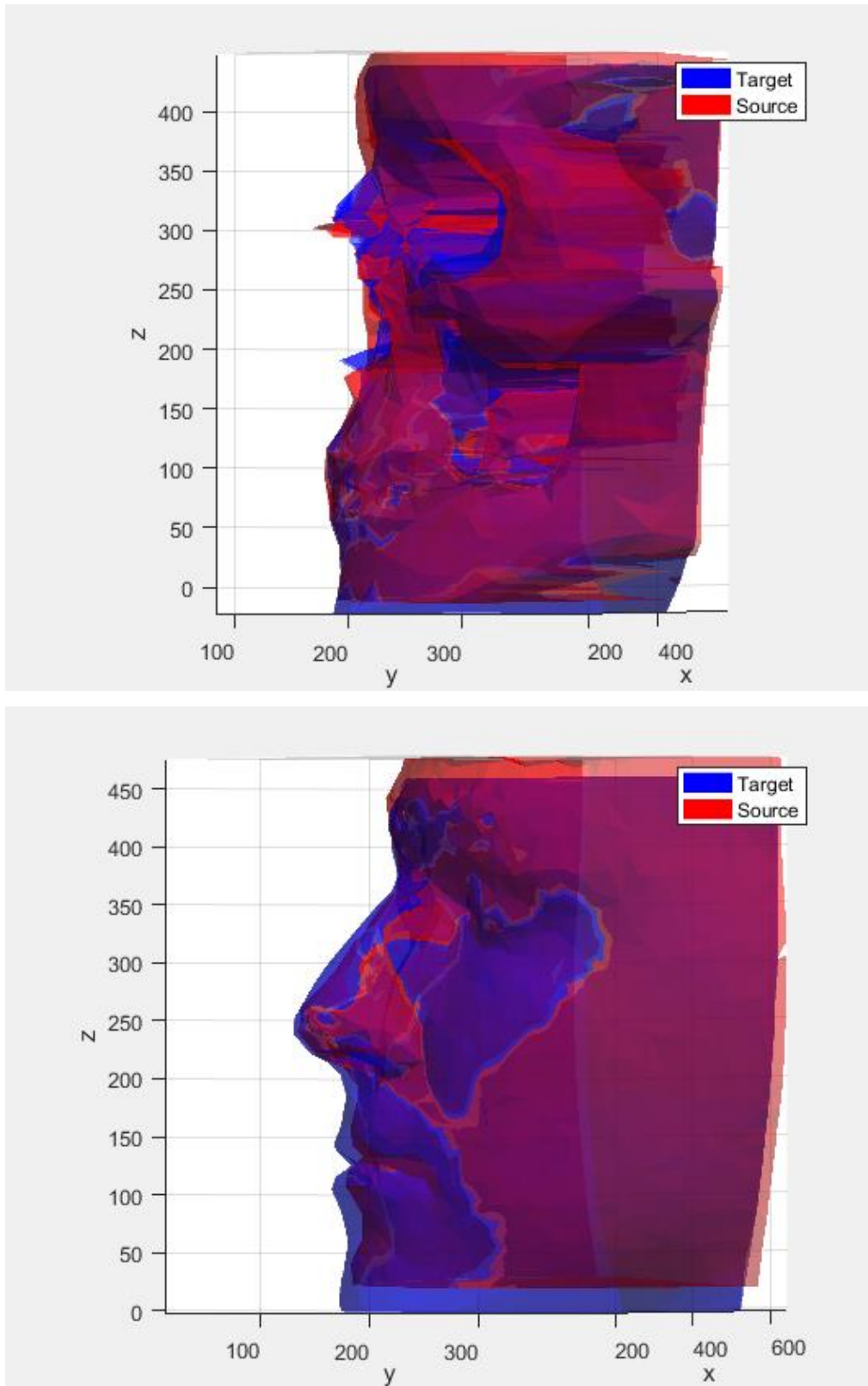


Figure 3-14: Meshes after Rigid ICP. (a) Source and target bone meshes after Rigid ICP
(b) Source and target skin meshes after Rigid ICP.

The reason why ICP alone doesn't work is because all the transformations are done globally and the template mesh is not actually taking the shape or features of the target mesh. This is why Non-Rigid ICP techniques is applied to deform the source mesh locally to the target mesh. Therefore, once the meshes are all aligned properly, the NRICP is conducted.

3.3.2 Optimal Step Non-Rigid Iterative Closest Point (NRICP)

The goal of the NRICP algorithm is achieved by first finding the relations to transform from the target vertices to the source vertices. Using these relations, the deformation is applied to the template and new vertices are created, after which are used iteratively to deform closely to the target.

NRICP is performed by recursively moving the template towards the target with decreasing stiffness. Unlike the Rigid ICP, NRICP performs more localized transformations to help shape the template mesh through the deformities of the target mesh. Simply put, the process of NRICP goes as follows: Each vertex in the template is considered and the preliminary correspondences on the target mesh are found with the nearest point search using the Hierarchical bounding spheres structure. The target is moved towards these preliminary correspondences with different stiffness values. The optimal deformations are determined depending on how flexible or stiff the mesh could be deformed. The stiffness weight starts with a larger value causing global alignment of the template mesh and decreasing the stiffness term further where the lower stiffness helps in more localized deformations. Once the deformation is performed on the template mesh, new vertices are captured. This new template's vertices are considered and the preliminary correspondences and later deformation is determined using a lower stiffness and the process continues iteratively with the newly created template meshes until the meshes converge, as shown in the Figure 3-15.

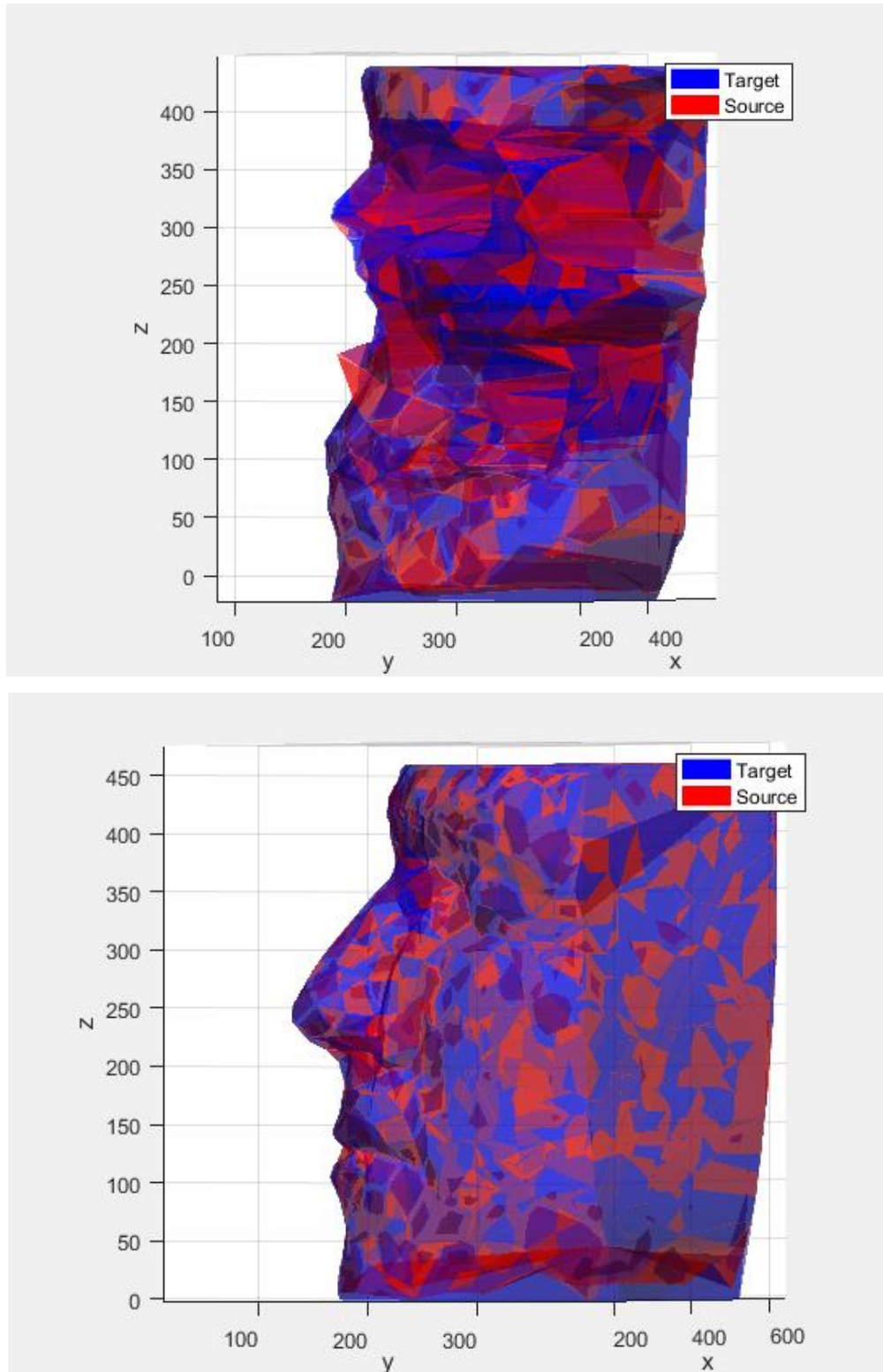


Figure 3-15: Meshes after Non Rigid ICP, completing the registration step. (a) Source and target bone meshes overlapped at the end of registration. (b) Source and target skin meshes overlapped at the end of registration.

In this process, the deformations are determined using a cost function which includes a distance function (E_d), a stiffness function (E_s) and a landmark function (E_l). The cost function is represented as follows (Amberg et al., 2007)

$$E(X) = E_d(X) + \alpha E_s(X) + \beta E_l(X)$$

The unknowns X are a $4n \times 3$ matrix, where n is the number of training samples.

$$X := [X_1 X_2 \dots X_n]^T$$

The distance function is used to force the distance between the template and target to be small and is represented as:

$$E_d(X) = \sum_{v_i \in V} W_i \text{dist}^2(\mathcal{T}, X_i v_i)$$

W_i represents the weight of the matched template vertices depending on the target vertices. The weight W_i is set to 1 if the template vertex finds a match with the target vertices and if there is not correspondence in the target vertices, then the template vertex weight W_i is marked as 0. v_i is the homogeneous coordinates of the template vertices which is in the form:

$$v_i = [x, y, z, 1]^T$$

Considering a point A and its closest point on the target, point B, $\text{dist}^2(A, B)$ represents the distance between A and B and the goal is to capture point B such that the distance between A and B is minimal.

The second term in the cost function that helps control the deformation of the template is the stiffness term. The stiffness keeps changing iteratively to generate global to localized deformations. This stiffness term is changed iteratively by constraining the weighted difference of the neighboring vertices transformation. The rotational and skew weighted difference γ in the weighted matrix G along with the difference of the neighbor's vertices transformation are used with a Frobenius norm. The γ value is set to 1 in our experiment. The stiffness term is represented by:

$$E_s(X) = \sum_{\{i,j\} \in \mathcal{E}} \|(X_i - X_j)G\|_F^2$$

for $G = \text{diag}(1,1,1,\gamma)$

The stiffness weight is given by α which changes with every iteration. The stiffness weight as the name says controls the stiffness and flexibility of the template mesh to deform around the target mesh. The larger the stiffness weight, the lesser the flexibility implying more global

deformation and the smaller the stiffness weight, the higher the flexibility resulting in localized deformations. Considering this strategy, the stiffness weights are taken in a decreasing order by first undergoing global deformations, for example fitting to the target mesh and later performing local deformations for taking the shape of the target. In this experiment, α is set between the range of 100 – 10, with 20 decreasing values of stiffness used for bone and 500 decreasing values of stiffness for skin.

The last term used in the cost function is the Landmark cost which can be used for correct initialization and registration. Adding these landmark terms makes the calculation easy as the equations are made quadratic. Using the landmark term helps find a local minima for a number of initial conditions, having quite a few points for collapsing the template mesh onto the target instead of having one point (global minima) on which the whole template mesh has to fall on, leading to correct initialization and registration. The landmark cost for mapping the template vertices onto the target is given as follows for a set of landmarks

$$\mathcal{L} = \{(v_{i_1}, l_1), (v_{i_2}, l_2), \dots, (v_{i_l}, l_l)\}$$

$$E_l(X) = \sum_{(v_i, l) \in \mathcal{L}} \|X_i v_i - l\|^2$$

The term β represents the landmark weight. By the end of the registrations, the landmarks considered are controlled using the landmark weight where the noisy point's priority keeps decreasing which ensures good initialization.

The new registration vertices are compared to the last iteration's vertices and if the difference is less than ε , the new iteration is considered as the final product from registration. Once the final registration is done and the deformed template mesh is captured for one Patient Scan, the vertices of the deformed bone and skin are saved, and the same procedure is continued for the remaining 47 scans. Using the above method, the skin and skull deformed meshes of all the scans are obtained. The registered vertices of the skull and skin are put together in a 1D array. The x, y and z columns of each skin and skull vertices are separately concatenated vertically as a 1D array. Each patient's new bone and skin 1D vertices are concatenated to the already existing skin and bone vertices array, forming 2 separate data structures of bone vertices and skin vertices. These newly formed skin and bone vertices are used in reconstructing an unknown face discussed in Section 3.4.

3.3.3 Registration Algorithm

The algorithm for the registration procedure is below:

- Initialize the template and target vertices and vertex normals.
- Perform Rigid ICP registration. Initialize the rotational matrix TR and translational matrix TT.
- For the iterations >50
 - Until the root mean square error is minimized.
 - ❖ Find the nearest neighbors of template mesh on target mesh.
 - ❖ Apply the transformation on template mesh and considered as the new source mesh. The optimal transformation matrix with the new fitted vertices.
- Perform Non-Rigid ICP registration for local deformations. Initialize the template vertex data, α and epsilon values.
- For each α , i.e. the stiffness $\alpha_i \in \{\alpha_1, \alpha_2, \dots, \alpha_n\}$; $\alpha_i > \alpha_{i+1}$ which is a decreasing order of α .
 - Until $\|X_i - X_{i-1}\| < \epsilon$, where X_i and X_{i-1} are the new and old deformations of the target vertices.
 - ❖ Evaluate preliminary correspondences for template vertices.
 - ❖ Consider these new preliminary correspondences for next iteration's deformation and find optimal deformations with changing α_i .

3.4 Reconstruction of Facial Data

Once the registered skin and bone vertices of all the scans are captured, the experiment can proceed to the reconstruction of missing data. As mentioned earlier, in 48 patient scans, 38 are used as training samples for the statistical method and the remaining 10 scans are used to testing purposes. For reconstruction, the experiment uses the reconstruction of missing data using Principal Component Analysis as mentioned in (Berar et al., 2005). The purpose behind using PCA is that it is good in capturing the variations in the database and considering sensitive data like facial data, this technique seeks n-dimensional basis which by maximizing the variance would also reduce the mean squared error. To start with, the training data is set up where all the registered

skin and bone vertices are grouped into different arrays separately. The registered bone vertices array B and registered skin vertices array S are formed with each column containing each scans bone and skin vertices respectively and all the columns being a multiple of 3 representing the sets of x, y and z axis locations of the vertices respectively.

$$B = [B_1 B_2 B_3 \dots B_n];$$

$$B_i = [x_{i1} y_{i1} z_{i1} x_{i2} y_{i2} z_{i3} \dots x_{in} y_{in} z_{in}]^T$$

Similarly representing the skin vertices as follows:

$$S = [S_1 S_2 S_3 \dots S_m];$$

$$S_i = [x_{i1} y_{i1} z_{i1} x_{i2} y_{i2} z_{i3} \dots x_{im} y_{im} z_{im}]^T$$

In the representation above, each column of B and S are the corresponding bone and skin registered vertices, i.e., B_2 and S_2 are the registered skin and bone of the same patient scan “Scan 2”. This concatenation is done later where the bone vertices and skin vertices are joined as follows.

$$X = [X_1 X_2 X_3 \dots X_{38}]$$

$$X_i = [B_i S_i]^T$$

This yields a $(3n+3m) \times 38$ matrix for X which contains all the training data with the registered bone and skin vertices. The dimensionality of the data is now $(3n+3m) \times 38$ which is very high and could affect the data analysis. For this reason, the dimensionality of the data is reduced while preserving its important properties (Zaki & Meira, 2014). To do this, the eigenvalues and eigenvectors of the covariance matrix of the centered vertices data is found. Using these eigenvalues and eigenvectors, the dimensionality is reduced by the following steps:

- Consider the eigenvalues $(\delta_1, \delta_2, \delta_3, \dots, \delta_r)$, sorted in a descending order as the largest eigenvalues are to be captured, and the eigenvectors $\theta = (\theta_1 \theta_2 \theta_3 \dots \theta_r)$ of the covariance matrix of centered vertices data where r is the present dimensionality of the data being $(3n+3m)$.
- Choose the smallest d such that $f(d) \geq \alpha$ where α is 0.95 that would help capture the largest eigenvalues with the most variation.

$$f(d) = \frac{\sum_{i=1}^d \delta_i}{\sum_{i=1}^r \delta_i} \quad \forall d = 1, 2, 3, \dots, r$$

- The reduced basis $\theta = (\theta_1 \theta_2 \theta_3 \dots \theta_d)$, a $(3n + 3m) \times d$ matrix is extracted which is further used in the missing data reconstruction.

Once the reduced eigenvector or the reduced basis is found, the missing data is reconstructed using least square method. Since our dimensionality d is always $<n$, the problem is solved using least square approximation with missing data. The data is solved as the following optimization problem

$$\text{minimize } \|Ax - B\|_F^2$$

Considering the equation from [Berar], the data is constructed into 2 matrices A and B, A being the independent variables and B having the dependent variables. Using these 2 matrices, the regression coefficients and the missing data are evaluated which would minimize the squared error between the model Ax and the dependent variables B [Alex William, website]. The two matrices as constructed as below

$$A = \begin{bmatrix} \theta_{1,1} & \cdots & \theta_{1,d} & 0 & \cdots & 0 \\ \vdots & \vdots & \vdots & \vdots & \vdots & \vdots \\ \theta_{3n,1} & \cdots & \theta_{3n,d} & 0 & \cdots & 0 \\ \theta_{3n+1,1} & \cdots & \theta_{3n+1,d} & -1 & \cdots & 0 \\ \vdots & \vdots & \vdots & \vdots & \ddots & \vdots \\ \theta_{3n+3m,1} & \cdots & \theta_{3n+3m,d} & 0 & \cdots & -1 \end{bmatrix}$$

where A is $(3n+3m) \times (d+3m)$ matrix which contains all the independent variables, which are the eigenvectors, zero matrix of size $3n \times 3m$ and a diagonal matrix of size $3m \times 3m$. The matrix B contains the bone vertices of the Patient scan whose skin vertices are to be reconstructed. As the problem is to minimize the square error and find the optimized fitting points for the bone vertices considered, the skin vertices are set to zero and the whole B matrix is centered with all the vertices mean, thus appearing as below

$$B = \begin{bmatrix} b_{i,1} - \bar{V}_1 \\ \vdots \\ b_{i,3n} - \bar{V}_{3n} \\ -\bar{V}_{3n+1} \\ \vdots \\ -\bar{V}_{3n+3m} \end{bmatrix}$$

where $b_{i,1}, b_{i,2}, \dots, b_{i,3n}$ are the bone vertices of the patient scan whose skin vertices are to be reconstructed and $\bar{V}_1, \bar{V}_2, \dots, \bar{V}_{3n}, \dots, \bar{V}_{3n+3m}$ is the mean of the all vertices of all the 38 patient test data.

Once the A and B matrices are constructed, the x is solved for using the Matlab's least square solution to solve the system of equations, `mldivide ()` (MathWorks `mldivide`, 2016).

x would be a $(d+3m) \times 1$ matrix with the optimized coefficients and skin vertices reconstructed using the A and B matrices that is in the form

$$x = \begin{bmatrix} C_1 \\ \vdots \\ C_d \\ s_1 \\ \vdots \\ s_{3m} \end{bmatrix}$$

The matrix x contains the regression coefficients C_1, C_2, \dots, C_d and the skin vertices s_1, s_2, \dots, s_{3m} of the skull/bone vertices, therefore reconstructing the unknown skin data. The unknown face that has been reconstructed is generated with a particular BMI, at a particular age, which is 19-35 years that has been restricted. A few samples of reconstructed faces, both front and side views are shown in Figure 3-16 and Figure 3-17:

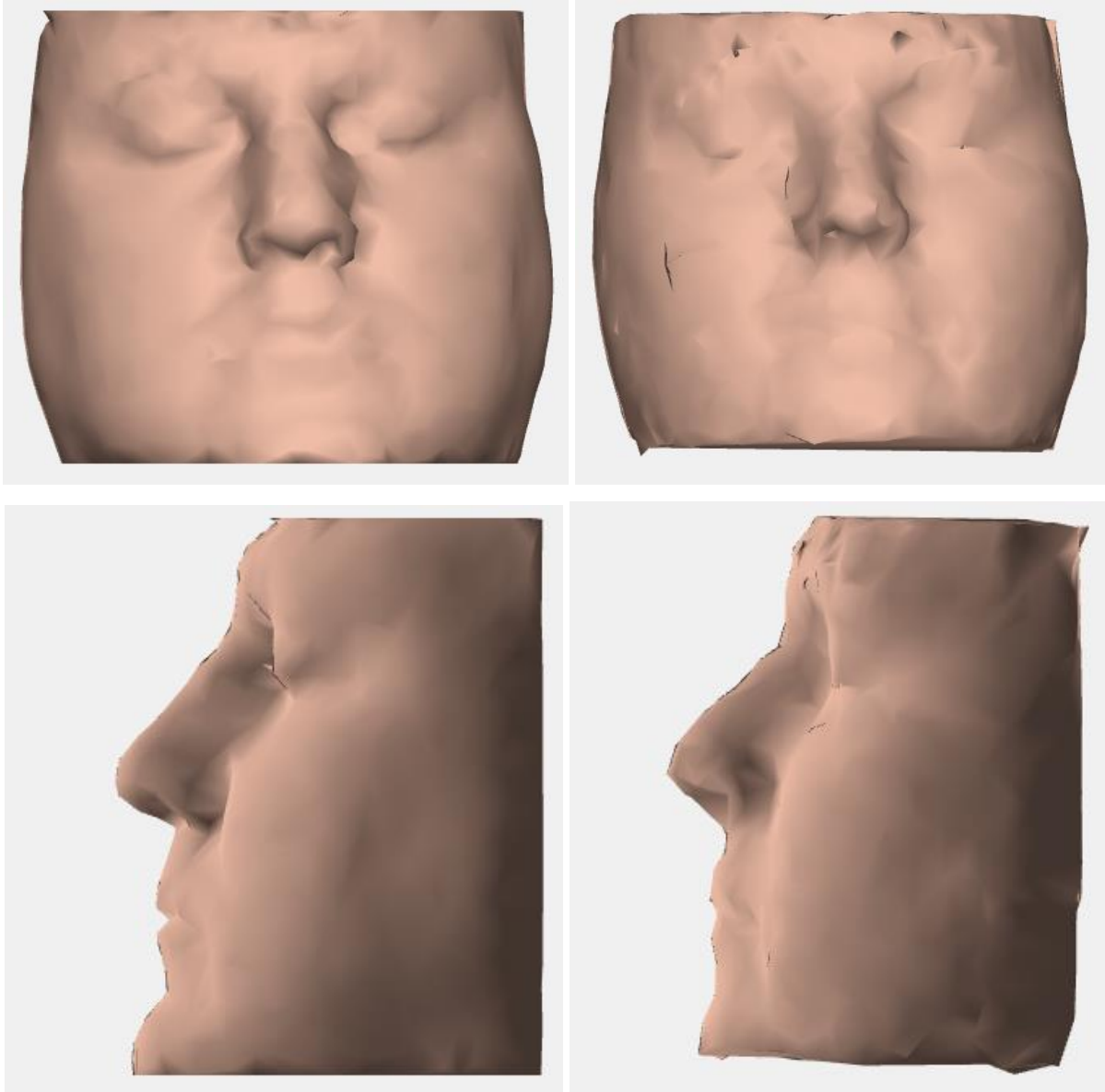


Figure 3-16: Original and reconstructed faces of one test data. (top-left) Original face of the test data, frontal view (top-right) Reconstructed face of the test data, frontal view (bottom-left) Original face of the test data, side view (bottom-right) Reconstructed face of the test data, side view.

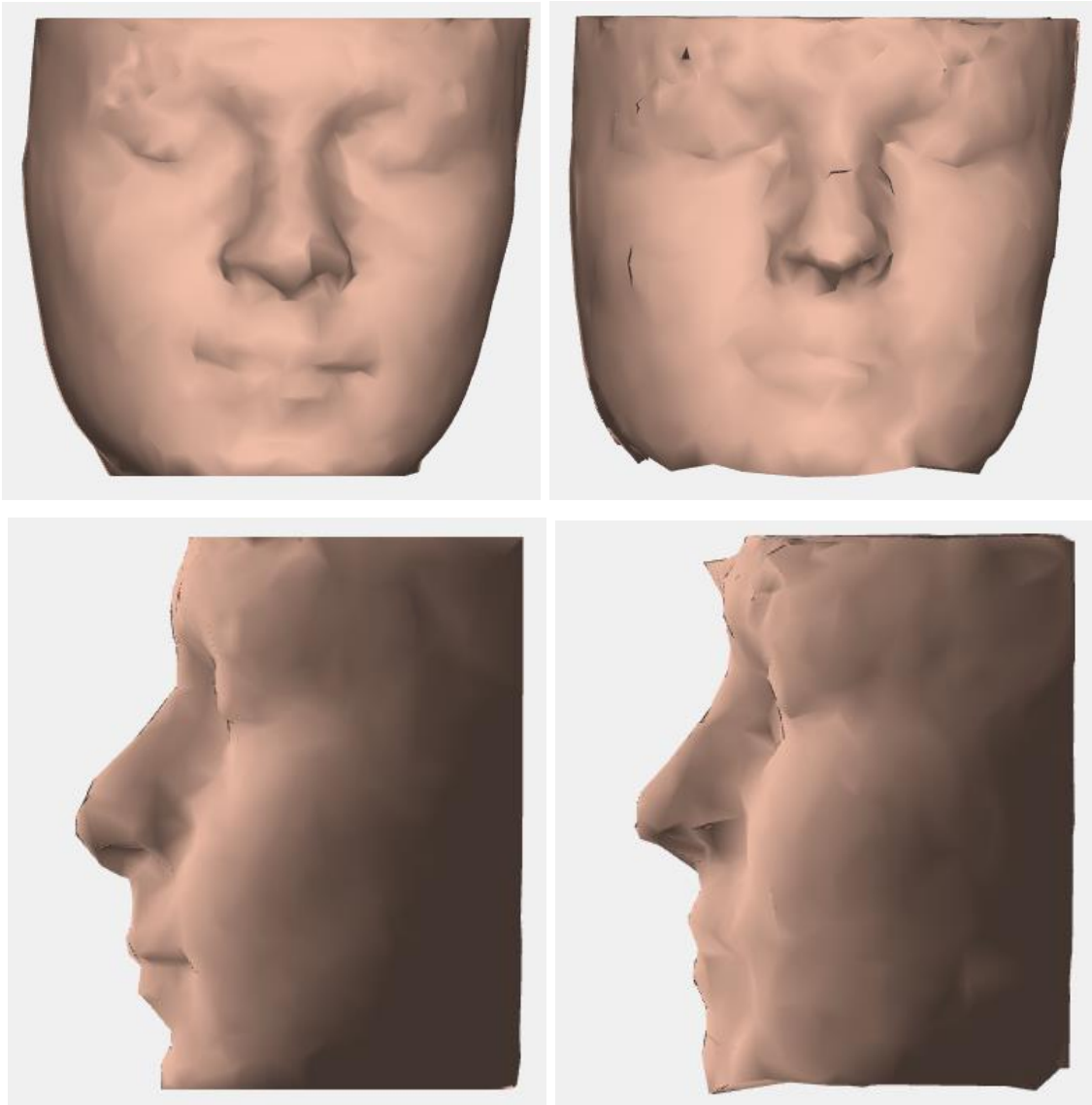


Figure 3-17: Original and reconstructed faces of one of the test data. (top-left) Original face of the test data, frontal view (top-right) Reconstructed face of the test data, frontal view (bottom-left) Original face of the test data, side view (bottom-right) Reconstructed face of the test data, side view.

As mentioned earlier, the face appearance changes at different ages and at different BMI's and this is addressed in the next section. A range of potential faces are generated at different ages and BMI levels for each particular skull making the identification more straightforward. This would be a whole other process that can only be done once the reconstructed faces are generated and the next steps of the experiment are conducted using the reconstructed face and its corresponding skulls.

3.5 Facial Appearance Transition with Physical Variants

After reconstructing the face using above methodology, the results can be used for identification purposes. But this would sometimes lead to false positives or missed identifications, as the person's age and BMI captured by the algorithm are represented at a certain range. A person could have interacted with many people since childhood and many of these acquaintances might recognize the person, when he was at a particular age or at a particular BMI. For example, consider John who had a friend Alex from college whom he hasn't seen for more than 10 years. When met after a long time (considering one of the friends has put on weight), it could be hard to recognize due to the changes in the physical appearance of his face. Similarly, if John is presented with a latest picture of Alex, it could be a little difficult for John to recognize Alex. But if he had a way to identify the face of the same person at a particular age or at particular body mass index he remembered, it would help in easy identification. In the example mentioned above, if John had to identify Alex and he remembers Alex to be thin at the age of 25, but the image that he was presented to was of a person with similar appearance or if it was a picture of Alex with a completely different appearance, it would either lead to false positives or false negatives respectively. In such situations, if the person is presented with the reconstruction of the face as he remembered, being at a particular age or thickness, portraying the changes in the image, it would help lead to a correct identification. This ideology is what is used in the second phase of our experimentation.

Instead of directly presenting the reconstructed face for identification, the appearance of the face is changed depending on the examiners request of how he remembered the person to be. An interactive platform is presented where the reconstructed face is presented with two sliders, one for changing the age and the other for changing the BMI of the reconstructed face and a reset button that will portray the original reconstructed face undoing all the changes made to the face.

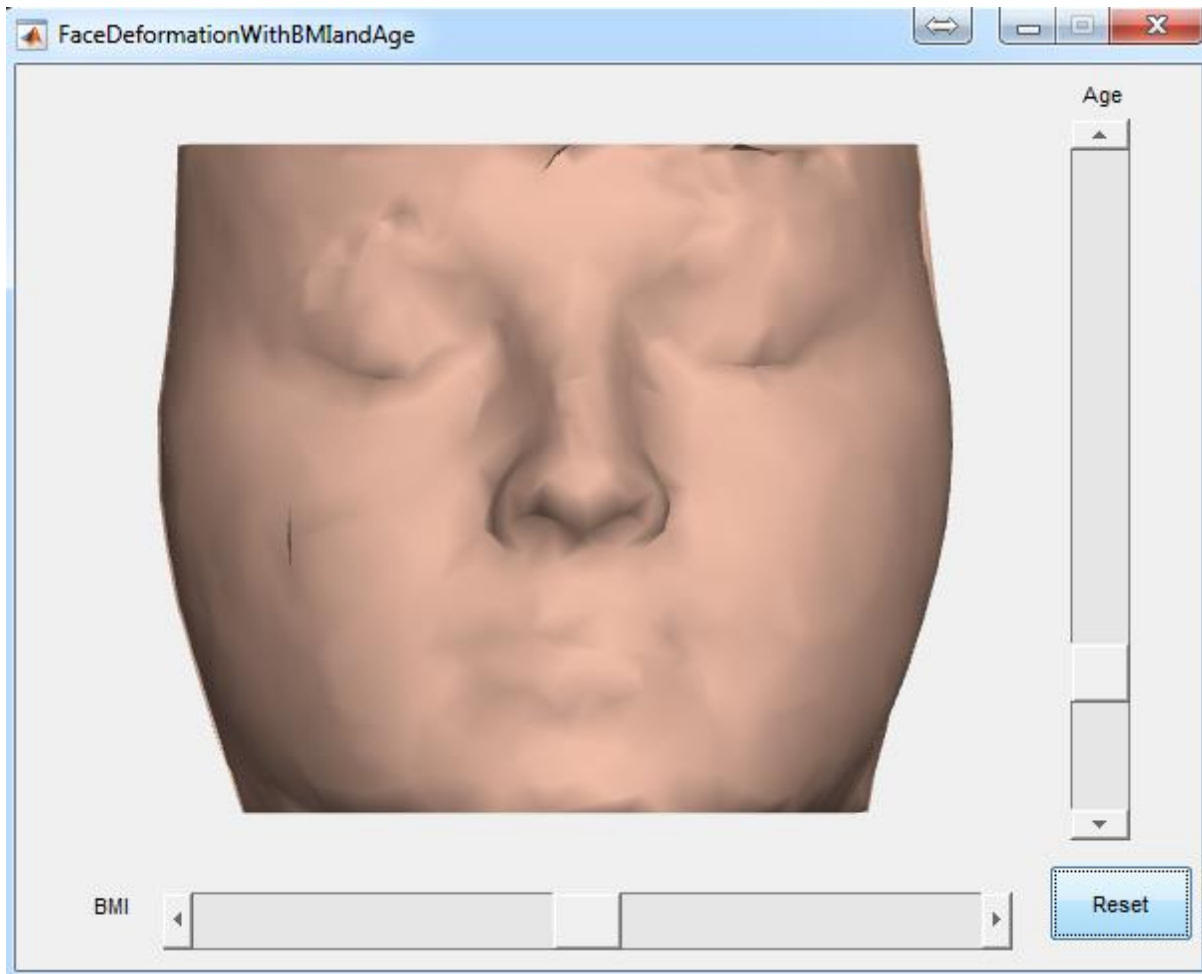


Figure 3-18: Interactive interface for observing facial changes depending on age and BMI.

As mentioned in 1.3, an interactive model is created for visualizing the appearance changes in the face due to age or BMI. This interactive model is a Matlab GUI window, which contains 4 separate blocks that help in visualization as shown in Figure 3-18. The first block is to display the reconstructed 3D skin mesh that is also used to show the changes in the appearance of the face, whose default value is the original reconstructed face. Two sliders control the values of the age and BMI parameters and the effect is reflected in the rendered face shape. In the implemented GUI, the horizontal slider controls the BMI value and the vertical slider controls age. The BMI slider ranges between -15 to +15 with a default value of zero. The positive values for BMI represent increase in the weight or Thickness of the face and the negative BMI values represent the decrease in the body weight from the initial default thickness. The age slider ranges between the values -15 and 70 with a default value of 0. The positive values represent increasing age and the negative

values represent decreasing age from the original value. The last block is a button for resetting and clearing all the changes made to the reconstructed skin mesh. Once any of the slider position is changed, a trigger is raised and the `Output_Fcn` for each of these changes are called. As the BMI and age slider positions are changed, the new slider values are logged, calling the `FaceDeformation Function`.

3.5.1 Evaluating Face Thickness Changes

The main concept considered for this processing is the changes in the face thickness at different ages and BMI's. A few points show much more difference than the other points in the face during aging or losing and gaining weight. For example, as the BMI increases, the inferior malar or the cheeks have more thickness difference than the supraorbital or the forehead but both of these changes are very critical to predict the final shape of the face. These crucial points are marked on the model skull mesh and the corresponding skin intersection points are calculated, assuming the changes in the thickness are in the normal direction of the vertex. Once the skin points are obtained, the mean square errors are calculated using the age and BMI and this error is added to each of the vertex position leading to a new set of skin points. These new set of skin points are used to manipulate and displace the neighboring unmodified vertices, creating a whole new set of skin vertices that generate a new face for the new age and BMI.

Before beginning the processing for facial deformation, these crucial points have to be marked on the skull. Since our model considers triangulation mesh for representing the surface and this triangulation surface comprises of triangles which are represented by faces and vertices, any point on this surface can be represented by the face index or its corresponding vertex. As we are interested in marking a point on the surface, the vertex index is used for marking these crucial points on the model skull. These vertices are used as markers for labelling these important points on the skull. The vertices marked are going to remain the same all over the samples as all the skull and skin meshes have been registered from the model skull and skin during the registration step. The positions that are to be marked on the skull are gathered from (De Greef et al., 2006). There are a total of 52 crucial points that are mentioned in (De Greef et al., 2006) but due to limited data availability, our experiment is considering 47 crucial points for facial deformation.

Table 1: TABLE for vertex markers (De Greef et al., 2006)

Landmark Number	Landmark Name	Landmark Description	Landmark Vertex
1	Supraglabella	Most anterior point on midline	560
2	Glabella	Crosspoint between midline and supraorbital line	498
3	Nasion	Midpoint of the fronto-nasal suture	528
4	End of nasal	Passage between bone and cartilage of the nose	509
5	Mid-philtrum	Centered between nose and mouth on midline	538
6	Upper lip	Midline on the upperlip	505
7	Lower lip	Midline on the lower lip	506
8	Chin-lip fold	Midline centered in fold chin, below lips	478
9	Mental eminence	Centered on forward most projecting point of chin	501
10/29	Frontal eminence	Centered on eyepupil, most anterior point of the forehead	855/ 173
11/30	Supraorbital	Centered on eyepupil, just above eyebrow	866/ 176
12/31	Lateral glabella	Junction of the frontal, maxillary, and lacrimal bones on the medial bone of the orbit	612/ 421
13/32	Lateral nasal	Side of the bridge of the nose, horizontal just above the end of a vertical line with the inner canthus of the eye	624/ 402
14/33	Suborbital	Centered on eyepupil on eyepupil, just under inferior orbita margin	853/ 208
15/34	Inferior malar	Centered on the eyepupil, just under the zygomatic process	646/ 374
16/35	Lateral	Next to the most lateral point of the ala nasi	666/ 346
17/36	Naso-labial ridge	The prominence next to the Mid-philtrum	628/ 423
18/37	Supra canina	Vertically lined up with the cheilion, on the horizontal level of the Mid-philtrum	707/ 338
19/38	Sub canina	Vertically lined up with the cheilion, on the horizontal level of the Chin-lip fold	671/ 321
20/39	Mental tubercle anterior	Most prominent point on the lateral bulge of the chin mound	606/ 308
21/40	Mid lateral orbit	Vertically centered on the orbit, next to the lateral orbit border	926/ 67

Table 1 continued

22/41	Zygomatic arch	Maximum, most lateral curvature of the zygomatic bone	967/ 7
23/42	Lateral orbit	Lined up with the lateral border of the eye on the center of the zygomatic process	935/ 100
24/43	Supra M2	Cheek region, lateral: lined up with bottom of nose; vertical: lined up beneath lateral border of the eye	754/ 276
25/44	Mid masseter	Middle of the masseter, the halfway point between the supraglenoid and the gonion	899/ 69
26/45	Occlusal line	Border of the masseter, on vertical level of the cheilion	847/ 120
27/46	Sub M2	Below the second molar on horizontally lined up with Supra M2	765/ 265
28/47	Mid mandibular	Inferior border of the mandible, vertically lined up with Supra M2	777/ 200

The vertices considered as markers are presented in the fourth column of the Table 1 besides their landmark names and all these points plotted on the skull, with the triangulation is as shown in Figure 3-19.

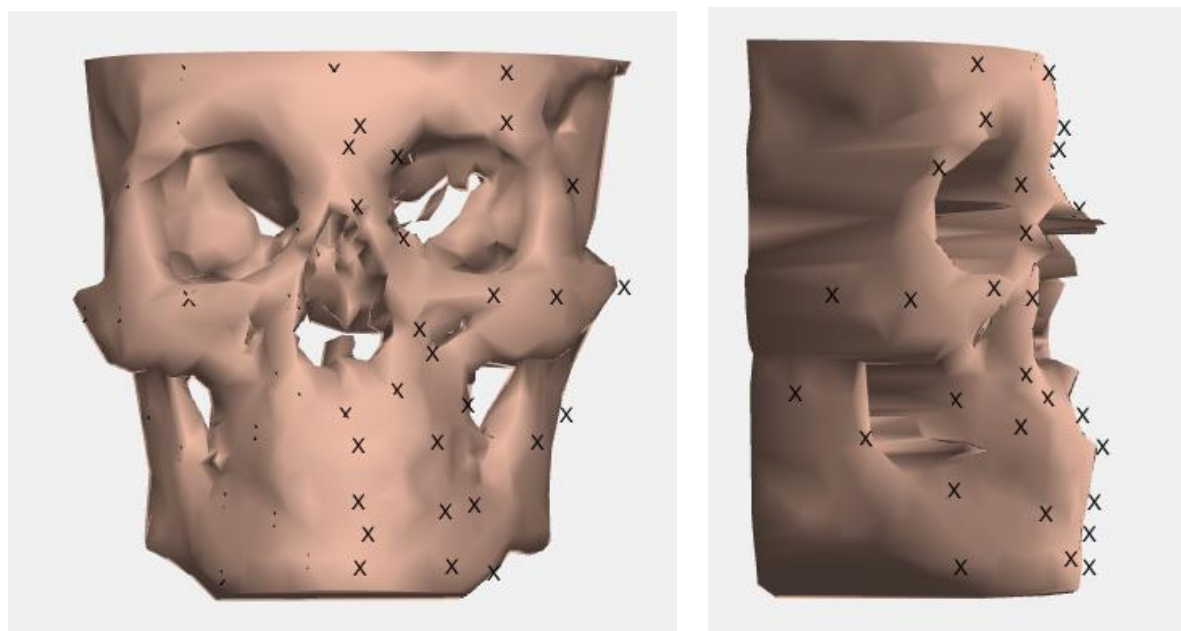


Figure 3-19: Model skull surfaces with vertex makers labelled as 'X' (a) Skull frontal view with vertex markers (b) Skull side view with vertex markers

Since we are interested in calculating the thickness from the bone to the skin and the data we have available are the vertex markers on bone, we calculate the corresponding intersection points on the skin with respect to these bone vertex markers. To calculate the corresponding skin points for the bone vertex markers, we consider the vertex normal of the bone vertex markers. A line is drawn in the direction of the vertex normal from the marked bone vertex and the intersection point on the skin is considered as the skin vertex marker as in Figure 3-20.

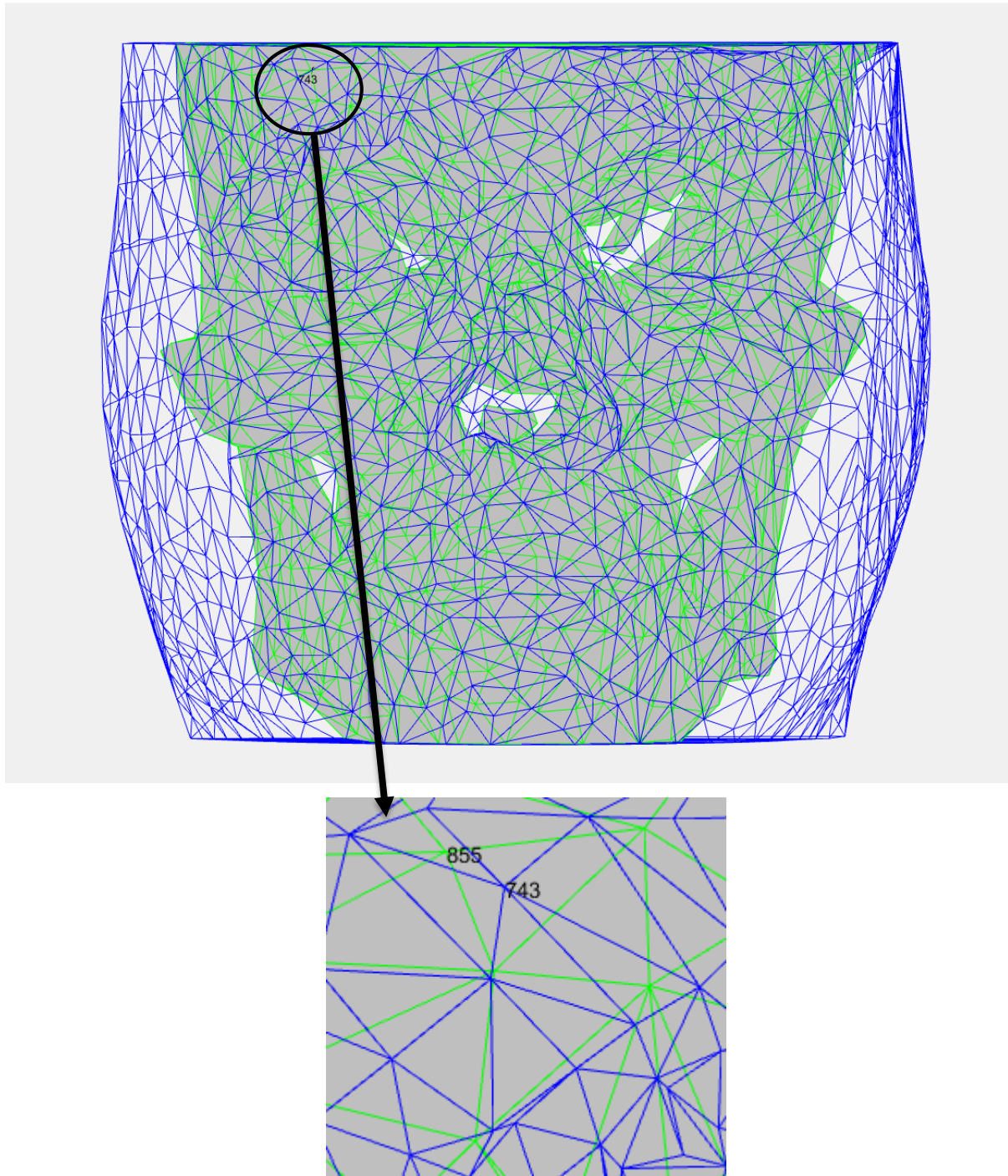


Figure 3-20: Bone and corresponding skin vertex marker. (top) Bone and skin mesh overlapped highlighting the bone vertex marker and its corresponding closest skin vertex. (bottom) Highlighted patch from the top image showing bone vertex marker [855] and its closest skin vertex [743]

3.5.2 Reshaping and Deformation

3.5.2.1 Skin Depths Evaluation for Reshaping

Once all the skin vertices corresponding to the bone vertex markers are calculated using the method above, the actual thickness at a certain age and BMI are calculated. The skin depths are calculated at different ages and BMI using the calculations below.

The new skin depths are calculated using the linear regression method mentioned in (Zhao et al., 2018). The change in the skin depths/ thickness are calculated using the formula below:

$$T = C_0 + C_1 * (age_{new}) + C_2 * BMI_{new}$$

where age_{new} , BMI_{new} are the reported changes from the interact C_0, C_1, C_2 are the partial regression coefficients whose structure is a follows:

$$C_0 = [c_0^1, c_0^2, c_0^3, \dots, c_0^{47}];$$

$$C_1 = [c_1^1, c_1^2, c_1^3, \dots, c_1^{47}];$$

$$C_2 = [c_2^1, c_2^2, c_2^3, \dots, c_2^{47}];$$

These coefficient values are obtained from (De Greef et al., 2006)paper that are showed in Table 2.

Table 2: Partial Regression coefficients at the selected landmarks

Landmark Number	Landmark Name	C_0	C_1	C_2
1	Supraglabella	2.7	2	62
2	Glabella	3.4	-2	77
3	Nasion	4.8	15	42
4	End of nasal	1.7	-2	36
5	Mid-philtrum	9.7	-39	39
6	Upper lip	10.6	-18	-21
7	Lower lip	10.1	-9	37
8	Chin–lip fold	7.9	23	54
9	Mental eminence	5.5	12	174
10/29	Frontal eminence	2.3	1	76
11/30	Supraorbital	3.3	0	95
12/31	Lateral glabella	4.9	-15	48
13/32	Lateral nasal	3.9	-14	10
14/33	Suborbital	7.7	-29	130
15/34	Inferior malar	12.3	6	249
16/35	Lateral	9.9	-32	14
17/36	Naso-labial ridge	9.6	-55	70
18/37	Supra canina	10.6	-57	20
19/38	Sub canina	9.2	-31	82
20/39	Mental tubercle anterior	6.6	8	129
21/40	Mid lateral orbit	4.1	-1	42
22/41	Zygomatic arch	3	-15	194
23/42	Lateral orbit	5.2	-44	266
24/43	Supra M2	22.5	-56	275
25/44	Mid masseter	13.4	-47	194
26/45	Occlusal line	13.1	-58	340
27/46	Sub M2	14.2	-27	250
28/47	Mid mandibular	3.8	12	329

Using these available coefficients, the changed age and BMI, the change in the skin depths are calculated. Once the difference in the skin depths are calculated, the modified skin depths/thickness is generated. As mentioned earlier, we consider the thickness difference to be affective in the direction of the vertex normal and therefore, these calculated difference in skin depths are added to the actual skin depths along the normal direction as below.

$$SV'_i = SV_i + (T * VN_i)$$

where SV'_i and SV_i are the new and old skin thickness at the i th bone vertex marker point respectively, before and after the modified age and BMI are applied, T is the thickness difference

calculated from the new age and BMI and VN_i is the skin vertex normal at the corresponding ith bone vertex marker point.

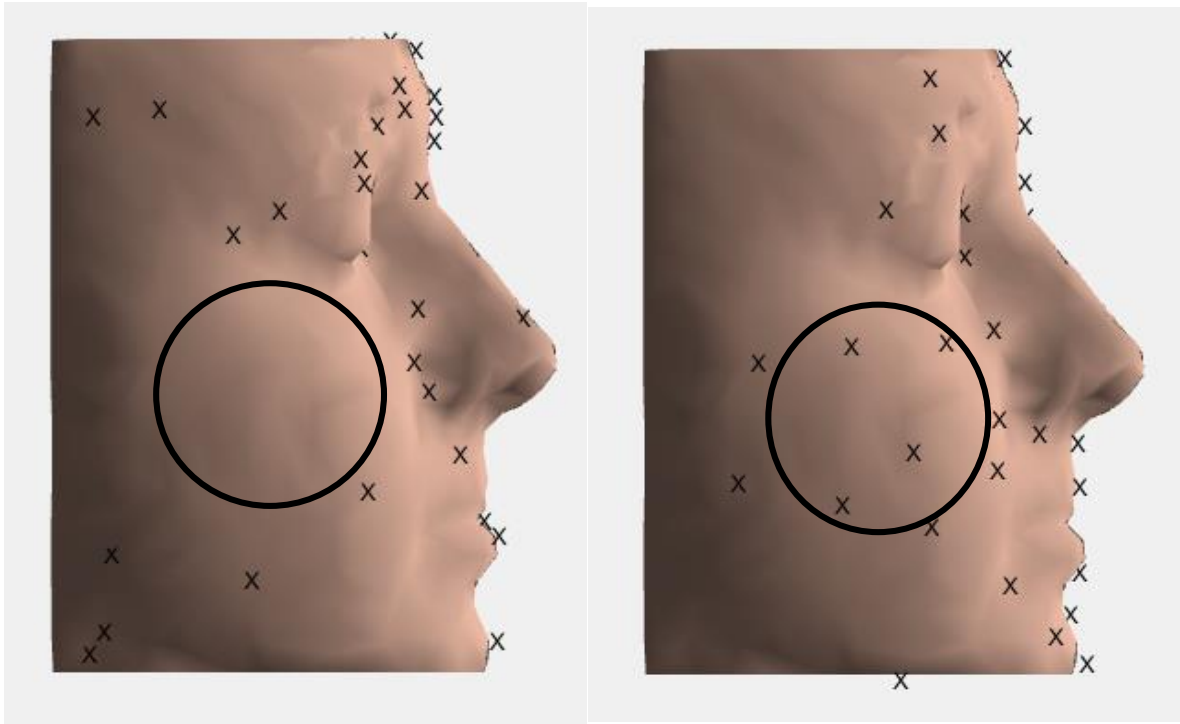


Figure 3-21: The above figures show the skin vertices (X) corresponding to the bone vertex markers before and after modifying with respect to the increase in BMI to 2. The figure (a) and figure (b), when observed has marked skin vertex points that are displaced depending on the thickness difference calculated.

3.5.3 Deforming Face Shape

Once the skin vertices corresponding to the bone vertices markers are calculated, the remaining skin vertices are calculated using these modified skin vertices. The remaining skin vertices are to be deformed depending on the already modified skin vertices and this is done using Laplacian Deformation method as mentioned in (Zhao et al., 2018) (Liao, Jin, & Zeng, 2012), which helps deform the surrounding vertices without hugely effecting the geometry of the surface and also preserving the already existing vertices. The deformed skin vertices are obtained using quadratic minimization problem as following:

$$A * x = B$$

where x , the deformed skin vertices that are to be solved for using A which is a topological Laplacian of the face mesh and B , being the Laplacian coordinate matrix (delta).

For calculating the A and B vertices to solve for x , we need the Laplacian matrices that are calculated as follows:

The topological Laplacian is calculated as below:

$$L = I - D^{-1}A$$

where A is the adjacency matrix of the skin vertices $S = \{S_1, S_2, S_3, \dots, S_n\}$, D is the degree matrix of the skin vertices and I is the identity matrix of size $n * n$. Once the Laplacian operator is calculated, A can be generated as follows:

$$A = \left[\begin{array}{c|c} \begin{bmatrix} 1 & \dots & 1 \\ \vdots & \ddots & \vdots \\ 1 & \dots & 1 \end{bmatrix}_{m*m} & \begin{bmatrix} 0 & \dots & 0 \\ \vdots & \ddots & \vdots \\ 0 & \dots & 0 \end{bmatrix}_{m*(n-m)} \\ \hline & L_{n*n} \end{array} \right]$$

where n is the number of skin vertices and m is the number of bone/skin vertex markers, which is 47 in our experiment.

The delta (δ) which is the difference between the vertex and the average of the neighboring vertices is calculated, and hence is known as the Laplacian coordinate of the vertex. As mentioned in (Sorkine et al., 2004), δ is not affected by translation but is affected by linear transformation, which makes it an ideal for consideration. Therefore, δ is calculated as follows:

$$\delta_i = S_i - \frac{\sum_{k \in NV_i} S_k}{D_i}$$

where S_i is the skin vertices and NV_i are the neighboring vertices at the i^{th} skin vertex and D_i being the degree of the i^{th} skin vertex. This δ is used to constructing B as follows:

$$B = \begin{bmatrix} [SV_1] \\ [SV_2] \\ [SV_3] \\ \vdots \\ [SV_m] \\ [\delta] \end{bmatrix}$$

where SV_i are the skin vertices with the modified thickness at the corresponding bone vertex markers.

Once the Laplacian matrices A and B are generated, x is solved using the quadratic minimization problem, for obtaining the modified face mesh at a certain age and BMI.

4. RESULTS

The outcomes and the results from the experimentation are shown in this section. We consider the validation of our results in two steps, one for facial reconstruction and one for facial appearance with BMI and age. Therefore, we discuss 2 sets of results for our whole experimentation.

4.1 Facial Reconstruction Results

The results from the facial reconstruction are measured quantitatively and qualitatively.

4.1.1 Quantitative Analysis

In quantitative analysis, we measure the mean squared error between the original face mesh and the reconstructed face mesh. The mean result of quantitative analysis of the reconstructed face meshes is 0.71 mm. All the reconstructed face meshes had an error less than 0.87mm. The majority differences were seen in the lips region, the lower cheek region and the eyes which constitute for the most error. But, we could not consider the quantitative analysis alone as the differences in the position of a few vertices on the nose or eyes can change the appearance of the whole face, which may not show a huge mean square error but when examined by looking at the face can seem completely different, hence leading to false identification. Therefore, we do a qualitative analysis for the results obtained to correctly verify and validate the results of the face meshes reconstructed.

4.1.2 Qualitative Analysis

For the qualitative analysis, we need to evaluate how well the reconstructed face reflects the actual face shape. This is evaluated by assessing the ease of recognizing the reconstructed face by human subjects. The qualitative validation is, therefore, designed with this goal in mind. In order to acquire the qualitative analysis results without bias, we conducted a live survey with people of different age groups and genders, to get the most reliable results.

The survey consists of 15 multiple choice questions. In each question the participants are presented with a reconstructed face at the top and a set of 6 images, all the original face meshes of different samples, where one of the images the original shape of the reconstructed face. The correct face is randomly placed among the 6 faces. The participants are asked to choose a face they think

that is a match to the reconstructed face mesh. This method of analysis is an attempt to duplicate the original forensic identification process, where a model of the face of the deceased is reconstructed and is shown to the relatives who would be identifying this reconstructed face. This survey was not a timed survey but was completed by the respondents in an average of 13 minutes. The survey was not restricted to any gender or age group. The respondent group consisted of men and women between the ages of 17 to 80 years. The survey participants were individuals from the general public, students from different departments and at different class levels, and staff from different departments. Most of them had minimum to no knowledge on the working of the algorithm and solely concentrated on picking the matches for the reconstructed image shown. All participants are almost always satisfied with the survey questions and no difference in satisfaction was found between young and older respondents.

The number of respondents who finished the survey successfully are 72, where 41 were female and 31 were male respondents. The age group break-down of the participants are tabulated as follows:

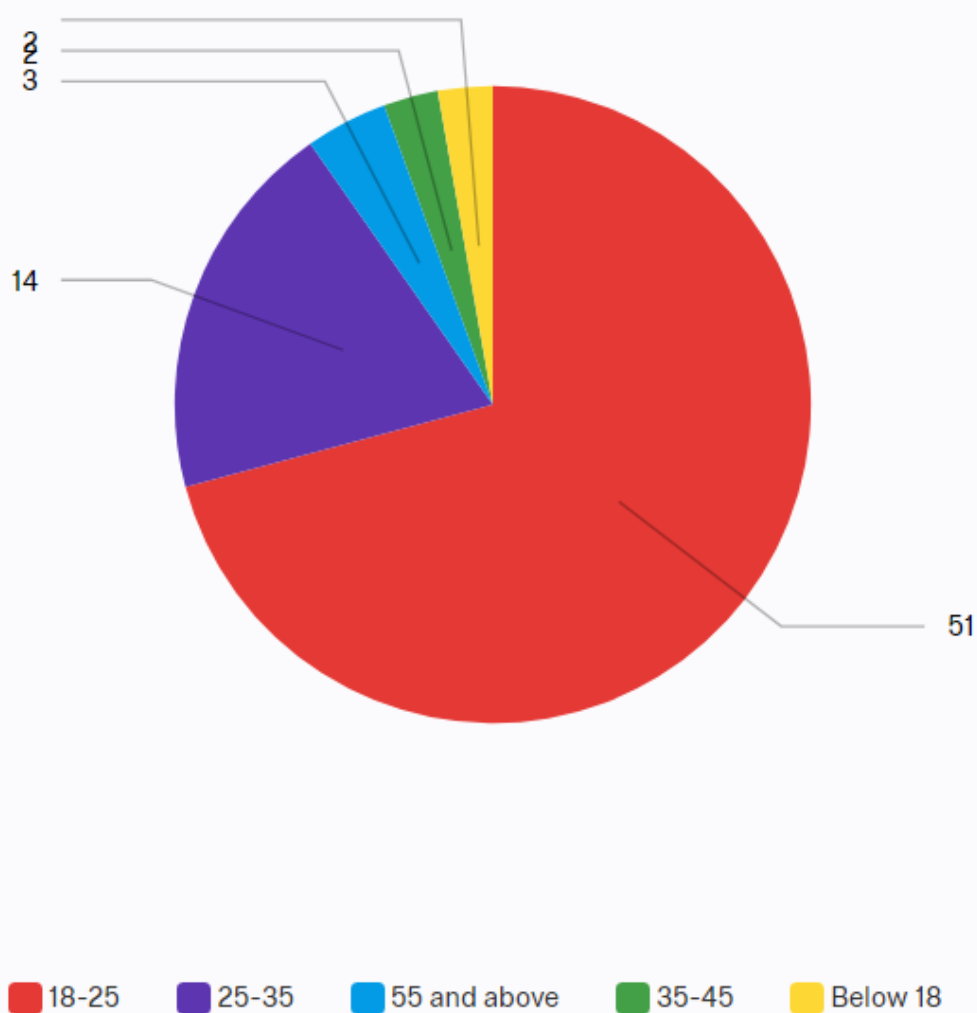


Figure 4-1: Pie chart showing the number of participants in each age group. The age group considered are given below.

In order to generate reliable results, the survey was always conducted using the same computer. The respondents are requested to come to the location where the computer is set up with fixed surroundings and were asked to take the survey, making sure that no other environmental conditions such as lighting, machine height, were changed. The computer is setup at eyelevel, placing the screen at an approximate distance of 70cm from the respondent. The survey computer is set up in a closed room with bright white lighting and this environment was kept unchanged. This survey is a new contribution to the facial reconstruction research area as most of the external

features that could affect the credibility of the survey are disregarded and the results are collected in a constant environment with unbiased approach towards verifying the algorithm with live respondents who have no knowledge in this area of research. Another unique feature is that this is the only computer aided 3D facial reconstruction algorithm using machine learning techniques that has been validated using a survey that contains 15 slides of different face pools that was taken by live respondents.

The idea for validating the algorithm using a live survey was taken from the paper (C. Wilkinson et al., 2006) who also validated their results of facial reconstruction generated by using the Manchester method of sculpting. They consider computer tomography data of males and females, place dowels on the skull and build the muscle and skin using Manchester method and generated 2 slides/posters of face pools for testing. These posters were shown to different individuals in different environments and are asked to match to one face in the pool. We try to use the same method but have simplified the approach by always having our surroundings constant and also considered 15 slides, more than 7 times the test sample size, which would increase the probability for effectiveness. Each slide, as mentioned earlier, has a reconstructed face that must be matched to one of the faces from the pool of images as shown in Figure 4-2:

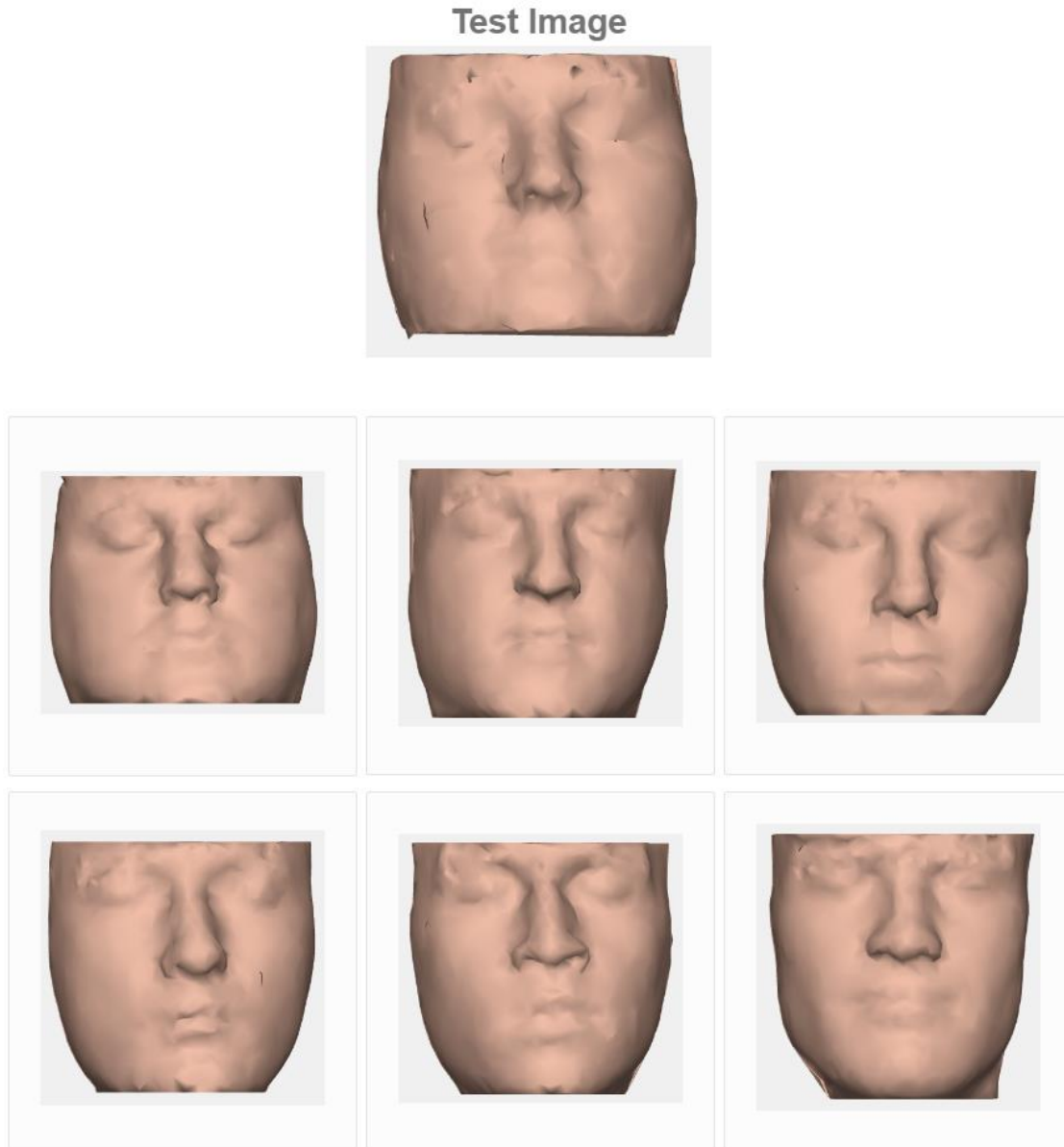


Figure 4-2: Slide 1. Top image is the test image which is also the reconstructed image that must be matched with one of the 6 images (2nd and 3rd row face pool). Click on one of the pictures from the face pool selects the respondent's choice.

As mentioned earlier, the survey was taken by 72 individuals, 41 being female respondents and 31 being male respondents. In the live survey conducted, the correct match expected for the reconstructed test image/question acquired the majority percentage in all the slides. The hit rate of the expected match in all the slides is almost always above 50% which is above chance. The

majority pick from the face pool from all the slides is always the expected face. One of the slides with the results is presented in Figure 4-3, Figure 4-4 and Figure 4-5.

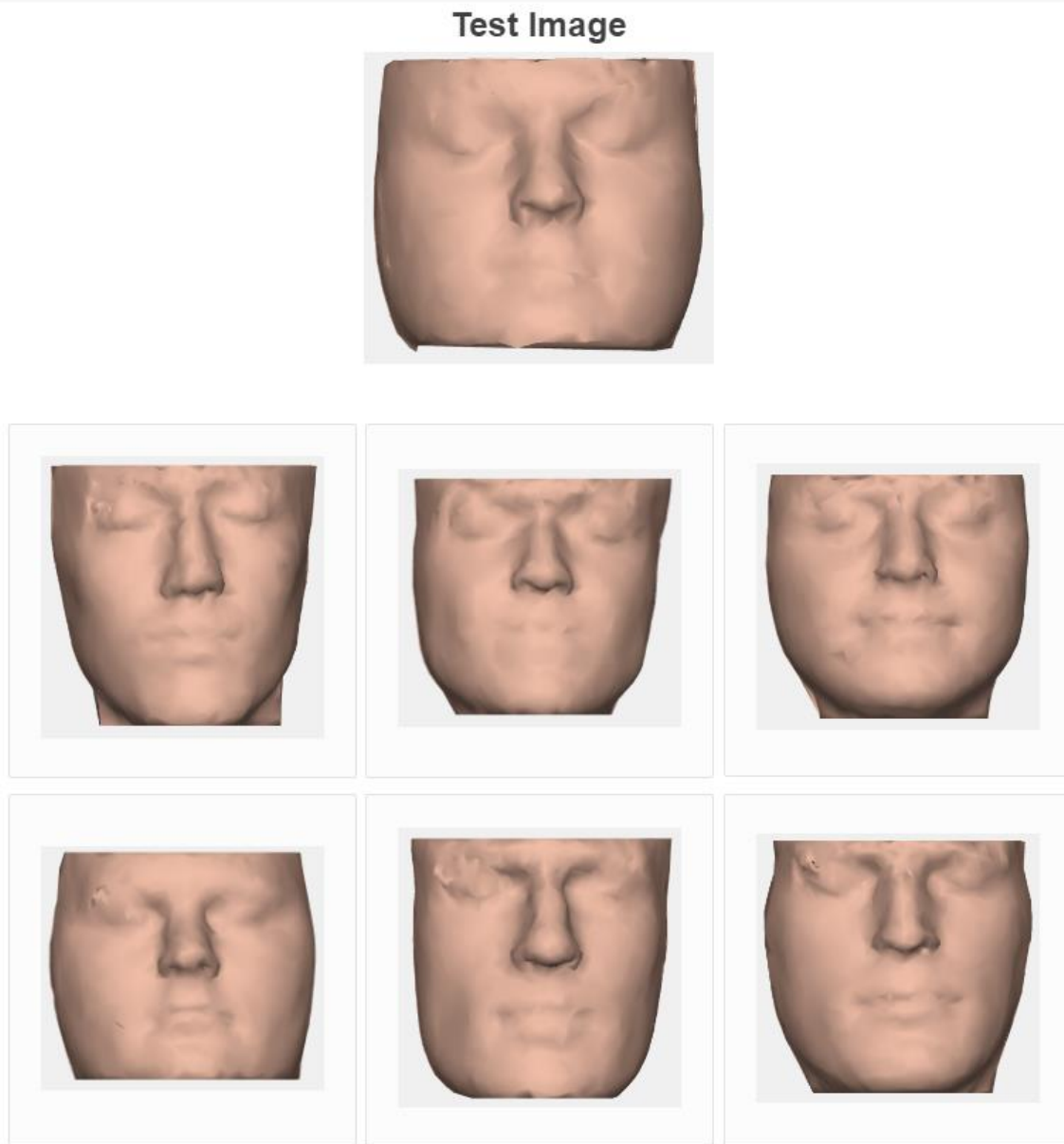


Figure 4-3: Slide 13. Top image in row 1 is the test image that is to be matched to one of the six images in row 2 and 3. The correct answer being the first image from left in row 3. The statistics are shown in the figures below.






#	Field	Choice Count
1		80.56% 58
2		8.33% 6
3		5.56% 4
4		2.78% 2
5		2.78% 2

Figure 4-4: A breakdown view of the responses report for slide 13. The top pick being the expected image with a hit rate of 58 responses that is picked about 80.56% when compared to other faces in the pool. If observed, the total count of responses is 72 for 5 faces where one face did not get a single response (first face from the left in row 2 in figure) showing majorly chosen face to be the expected answer.

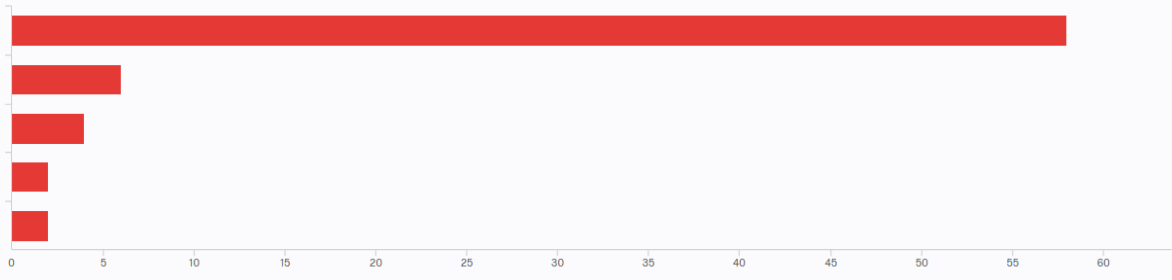


Figure 4-5: The bar chart of the choice count of the responses of slide 13 of figure. The most prominent bar being the expected face choice count from the live respondents.

The hit rate for all the slides, being the total count of respondents choosing the right answer and percentages of this hit count for all the slides are represented in Table 3.

Table 3: Hit rate of each slide in column 2, Choice count and the percentage of hit rate of each slide in column 3, Percentage.

	Choice count	Percentage (%)
Slide 1	65	90.28
Slide 2	32	44.44
Slide 3	48	66.67
Slide 4	40	55.56
Slide 5	43	59.72
Slide 6	37	51.39
Slide 7	58	80.56
Slide 8	60	83.33
Slide 9	42	58.33
Slide 10	44	61.11
Slide 11	48	66.67
Slide 12	47	65.28
Slide 13	44	61.11
Slide 14	49	68.06
Slide 15	31	43.06

More statistical analysis is done on the results in further sections where the survey and the responses are statistically evaluated by conducting reliability and validity testing.

4.1.2.1 Testing

The reliability and validity of the survey, as mentioned earlier, is also accounted for that measures how reproducible the survey data is. We conduct three tests each for the reliability and validity of the survey.

4.1.2.2 Validity Testing

Validity testing for a survey measures how well the survey is measuring the quantities that it is set out to measure. These measures are not particularly formulated or scientific methods but are rather used to validate the procedure with diligent assessment. In our case, the survey created has to measure how well the results from the algorithm can be useful for identification. To do this, we need to make sure the survey is actually comparing the same data and is setup in the form that could help decide the results obtained are accurate. The three tests of validity are:

4.1.2.2.1 Face Validity

Face validity as the name says is like a primary test that can be done to see if the survey is doing what it's intended to do. It is a cursory review done by unexperienced people and the feedback is used to change the survey accordingly. It is like a third opinion about the survey, making sure it's measuring the right value. In our case, a couple people from different departments who have no experience in Facial Reconstruction have gone through the slides before making the survey live. The goal of the survey is explained to these people and are asked to give feedback on how well the survey illustrates its tasks. This feedback is considered, and changes are made to the survey. The changes proposed were to increase the image size when we considered 10 images in 1 slide. Therefore, we considered 6 images per slide, preserving the features of the face image, hence improving the face validity of the survey.

4.1.2.2.2 Content Validity

Like Face validity, content validity is also a test that measures if the survey is measuring the correct value but it is a little complicated that is based on an expert's subjective opinion. This is a more organized way of reviewing the survey, which is conducted by a group of experienced individuals whose area of expertise matches with the one survey-related field. An in-depth analysis is done on the prepared survey and is checked if the survey has everything necessary for validating

the algorithm. In my case, Dr. Tuceryan and Dr. Kula reviewed the survey and forwarded the feedback with changes required. One of the things that was added based on the review is the reliability testing for the survey that increased the credibility of the algorithm and functionality.

4.1.2.2.3 Concurrent Validity

Once the survey is deemed to be working, a new step is added to check the validity which is by comparing the present test with an already existing, most reliable test and checking if they are assessing the right variable. In our case, we are comparing our survey against (C. Wilkinson et al., 2006) which talks about the surveys conducted before and how their measures accuracy. We consider this as our “gold standard” and built the survey accordingly, adding and improving the techniques on testing the accuracy of our functionality.

4.1.2.3 Reliability Testing

Like validity testing, we conduct a few tests for reliability of the algorithm and the survey. Reliability tests are used to check for the random error that could be difficult to compensate for as it is an unpredictable error. In order to compensate for these random errors, the below tests are done and if the correlation coefficient value falls below a certain number then we can conclude that the survey or the procedure have been returning ambiguous results. This is a statistical way of measuring how stable the survey and the algorithm is. The reliability test that we conducted are:

4.1.2.3.1 Test-Retest

In order to say that the survey created is reliable, a simple test that can be done is the test-retest where a slide is repeated with the same reconstructed face and the same image pool in the same order. The goal of this test is to measure the stability of the respondent and to measure the survey being our instrument to validation of our algorithm. The correlation coefficients are then calculated for the 2 observed slides and if the value is 0.70 or more then the values are considered to be good and the survey is considered reliable. To test the test-retest method in our survey, we created slide 1 and slide 8 with the same data, having the same test image and the same face pool in the same order as in Figure 4-6.



Figure 4-6: Slide 1 repeated as slide 8 in the survey.

The majority pick is the first face image from left in row 2 in both the slides being the expected correct answer. The choice count of the face pool for both the slides is shown in Figure 4-7 and Figure 4-8.









#		%	Choice Count
1		90.28%	65
2		4.17%	3
3		2.78%	2
4		1.39%	1
5		1.39%	1

Figure 4-7: Slide 1 face pool choice count and choice percentages.

#	Field	Choice Count	Choice Percentage
1		60	83.33%
2		4	5.56%
3		4	5.56%
4		4	5.56%

72

Figure 4-8: Slide 8 face pool choice count and choice percentages. The other 2 faces had 0 picks and so are not presented in the report.

The correlation coefficients when calculated for the choice counts of both the slides is equal to 0.9981 which is way above the 0.7 threshold for being considered reliable under test-retest condition.

4.1.2.3.2 Alternate Form

The second test that could measure the reliability of the survey and is also used to avoid the learning that happens to participants while going through these slides is the alternate form. Brain being an intricate organ that can do data mining and learning instantly when introduced to new content, it is a natural phenomenon to remember or recognize things that are been visited in the same order. But the same question when posed in a different order, requires the attention of the survey taker, which in turn measures if the survey is doing a good job in alternate form test.

This alternate form is tested using one of the 15 slides where the slide is repeated with one of the existing slides but is rearranged in a different order. We can check using this method if the respondent is answering the right choice even in difficult or changed conditions, proving the credibility of the survey. The correlation coefficients are calculated for both original and rearranged slides and if these values are high, the alternate form reliability of the survey is said to be good.

In the survey, to test alternate form reliability, slides 4 and slides 9 are used. The slides 4 and 9 are created using the same data with the reconstructed test image and the same pool of faces but the difference being the order of the face pool from slide 4 and 9. The face pool is rearranged in slide 9 which is used to conduct the equivalent form test. The slides 4 and 9 are shown in Figure 4-9 and Figure 4-10.

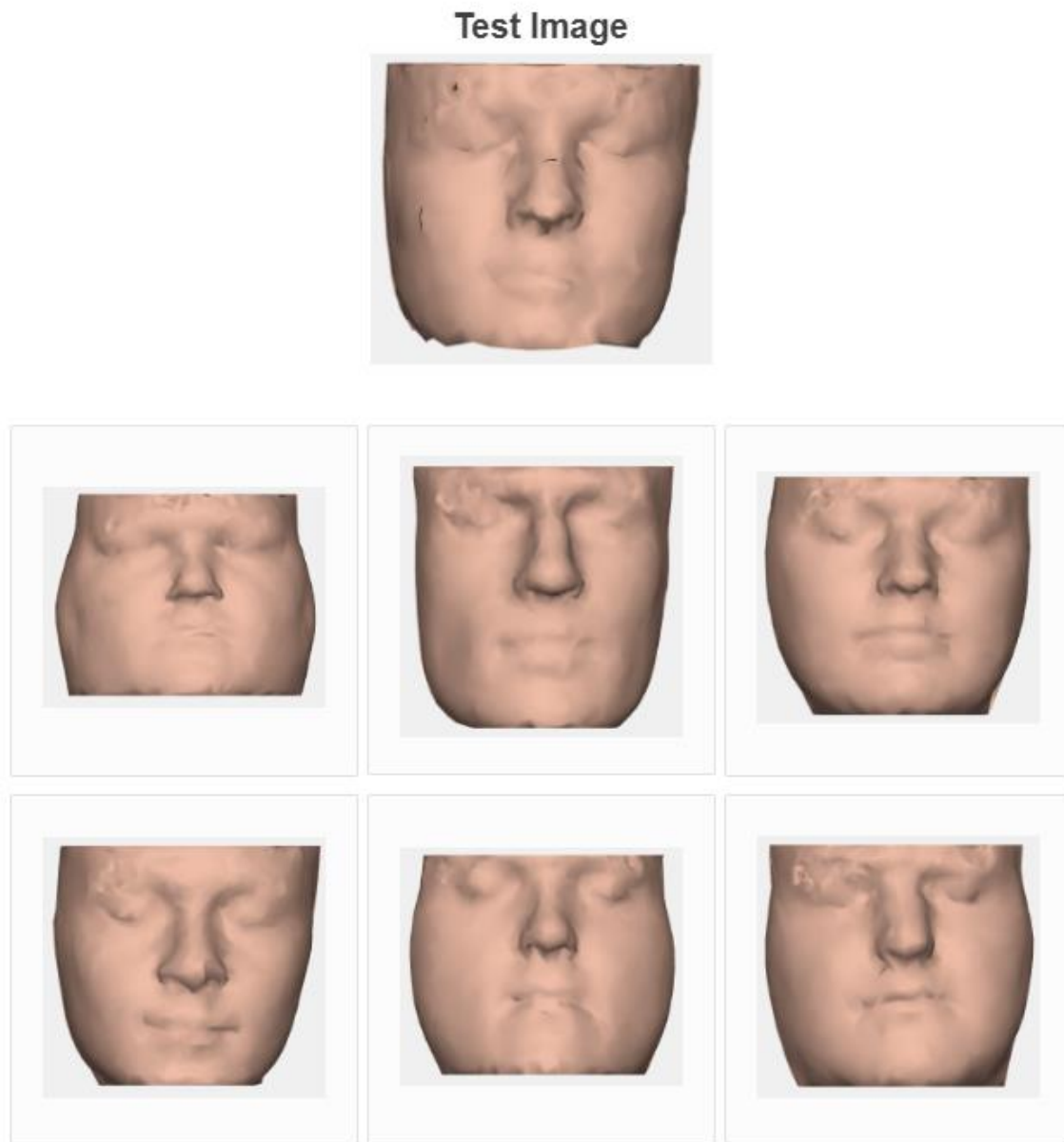


Figure 4-9: Slide 4 from the survey

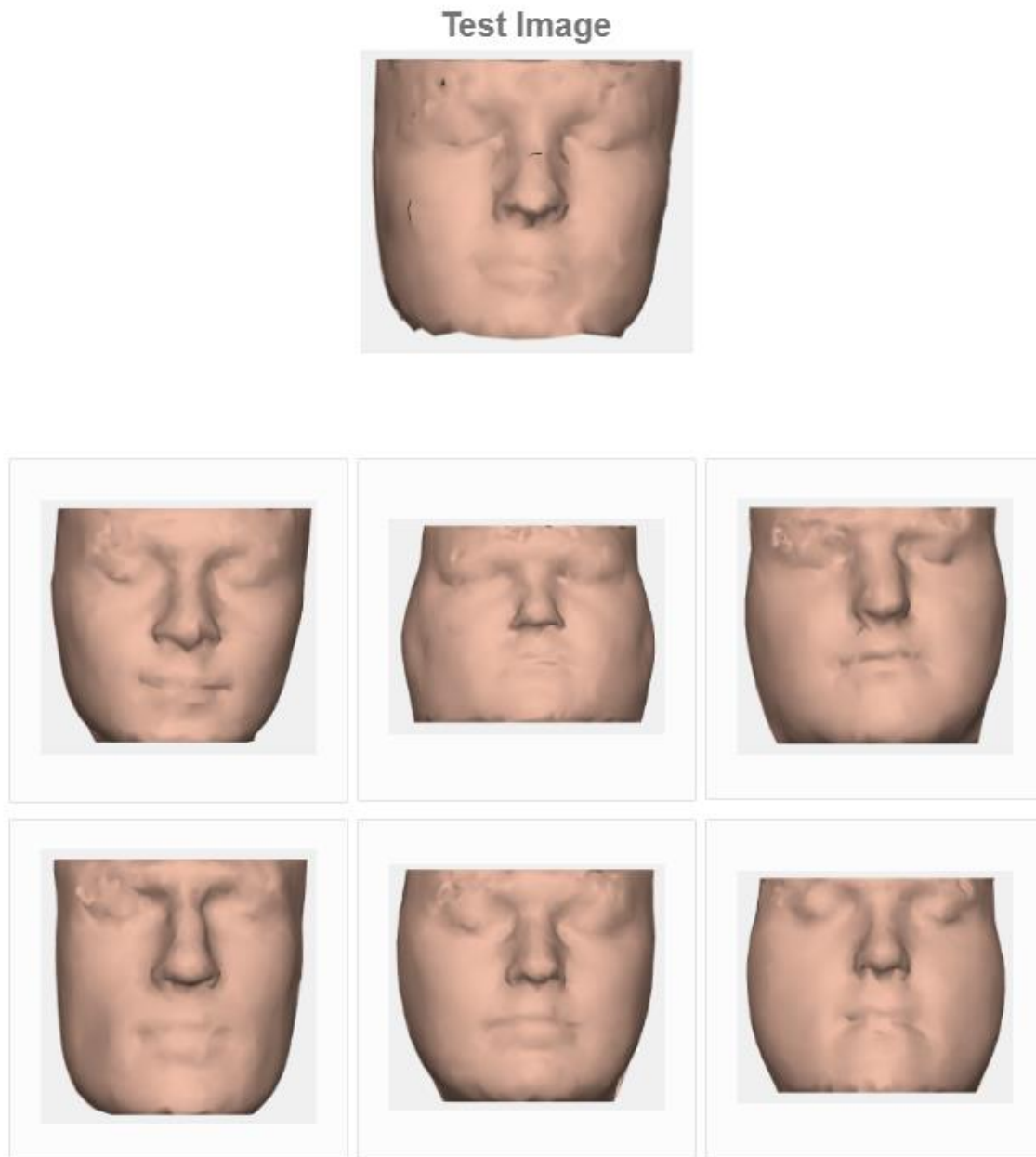


Figure 4-10: Slide 9 from the survey

The choice counts of both the slides are shown in Figure 4-11 and Figure 4-12.






#	Field	Choice Count
1		55.56% 40
2		25.00% 18
3		11.11% 8
4		6.94% 5
5		1.39% 1

Figure 4-11: Slide 4 Choice count and choice percentage for each face in the pool.






#	Field	Choice Count
1		58.33% 42
2		16.67% 12
3		15.28% 11
4		6.94% 5
5		2.78% 2

Figure 4-12: Slide 9 Choice count and choice percentage for each face in the pool.

The correlation coefficients when calculated between both the choice counts of slides 4 and 9 is 0.9652, proving the alternate form reliability of the algorithm and the survey.

4.1.2.3.3 Equivalent Form

We also test our survey for Equivalent form reliability which tests the equivalence of the survey by creating 2 slides with the same reconstructed face but with different pool of images, with one face amongst the pool being the correct original face mesh. The reason behind this test is to check if the survey created measures the same trait. This test of reliability ensures avoiding the learning from the slides previously filled. The correlation coefficient of both the original and the

changed slides are evaluated, and a high score signifies a good equivalent form reliability for the survey.

To test our survey for equivalent form reliability, two slides 11 and 15 are created in such a way that they are questioned to match the same reconstructed test image with a different pool of face images with one being the correct match to the test image. To simulate the environment similar to equivalent form reliability test, we considered this approach. The two slides are shown in Figure 4-13 and Figure 4-14.

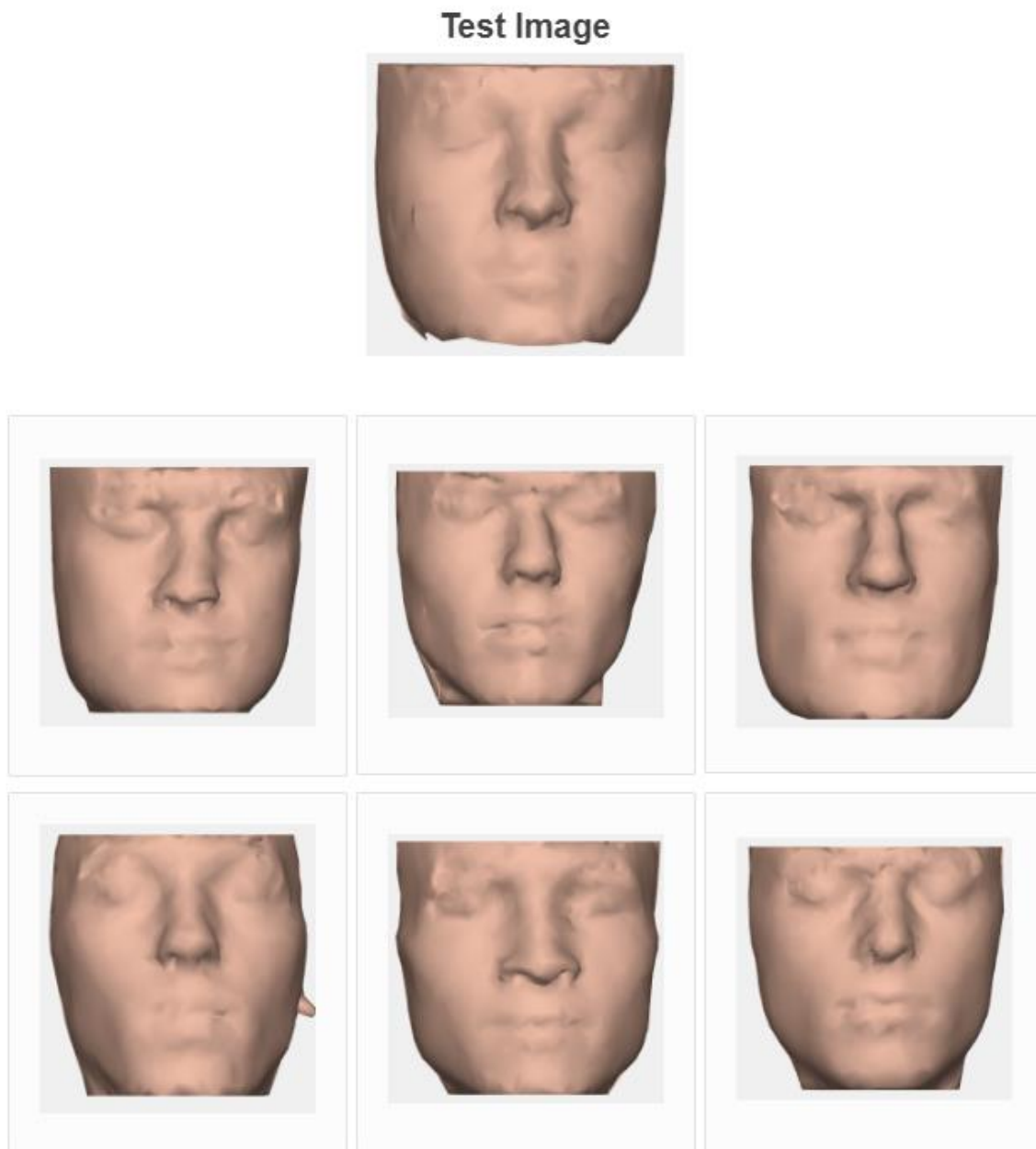


Figure 4-13: Slide 11 from the survey

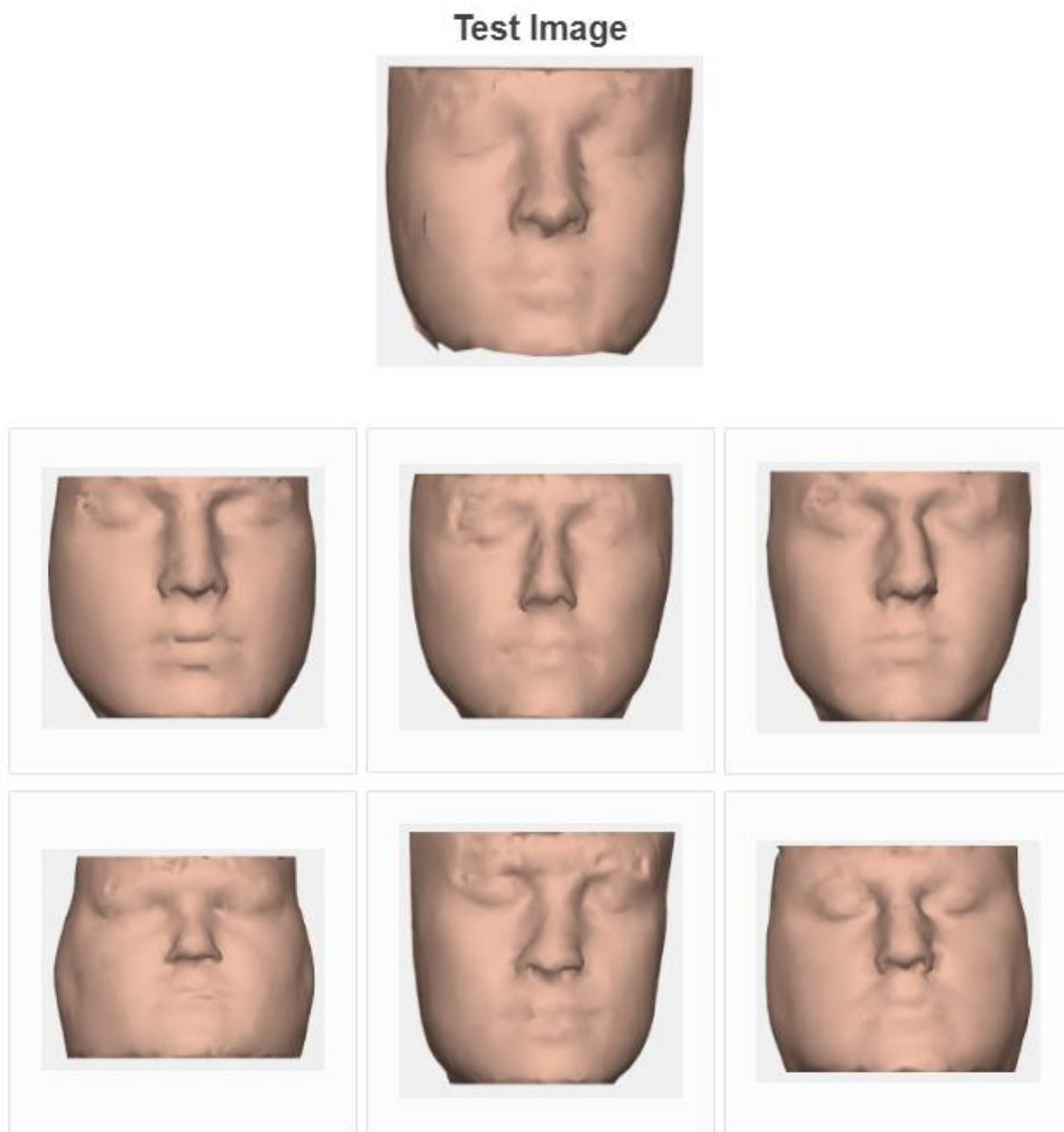


Figure 4-14: Slide 15 from the survey

The choice counts and choice percentages of the slides 11 and 15 are presented in Figure 4-15 and Figure 4-16, for correlation coefficient calculation.







#	Answer	%	Choice Count
1		66.67%	48
6		11.11%	8
4		8.33%	6
2		6.94%	5
3		5.56%	4
5		1.39%	1

Figure 4-15: Slide 11 Choice count and choice percentage for each face in the pool.






#	Field	Choice Count
1		43.06% 31
2		25.00% 18
3		15.28% 11
4		12.50% 9
5		4.17% 3

Figure 4-16: Slide 15 Choice count and choice percentage for each face in the pool.

The correlation coefficient when calculated between the slides 11 and 15 is equal to 0.8911 which also satisfies the condition for equivalent form reliability. These tests conducted on the survey have proved the reliability of the algorithm and hence testing our facial reconstruction algorithm with the live survey is considered as a golden standard for our algorithm.

These are the results and validation of the results for facial reconstruction. The results from the second phase of experimentation which is changing the facial appearance based on BMI and age are discussed in further sections.

4.2 Facial Appearance Change Results

The second phase of our experiment shows the physical facial appearance changes in the reconstructed face at different ages and different levels of BMI. These results are visualized and discussed in this section.

For the second phase, an interactive window is created that would allow the user to change the BMI and age of the reconstructed face. These changes are simultaneously incorporated, displaying the new face on the interactive window along with the new BMI and age information.

4.2.1 Illustration 1

This illustration shows the facial appearance when the BMI is changed. The illustration is done using the **Error! Reference source not found.** below:

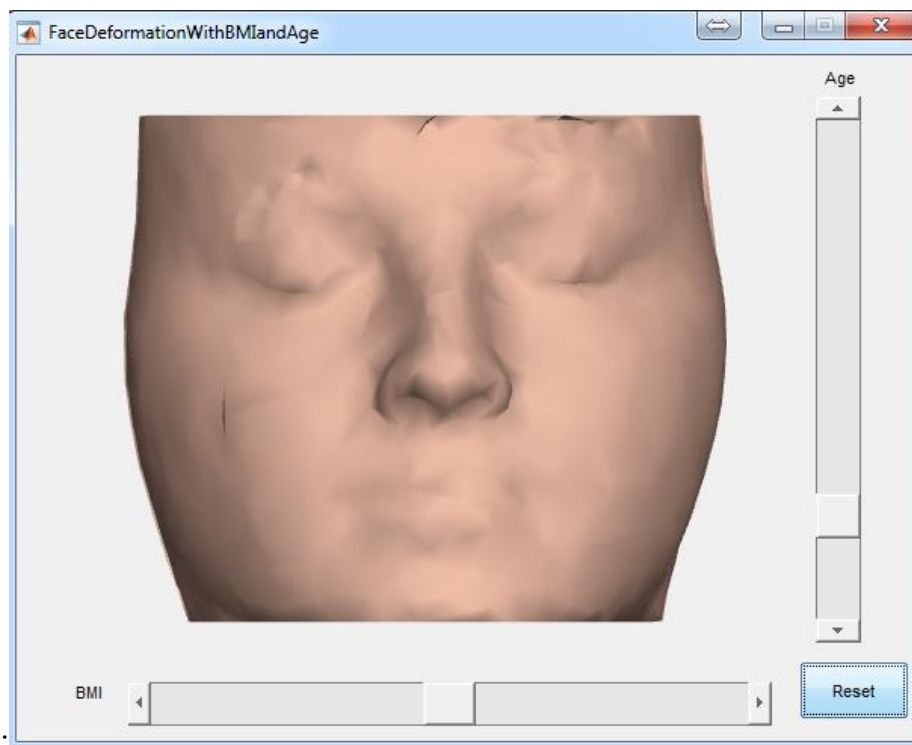


Figure 4.17 continued

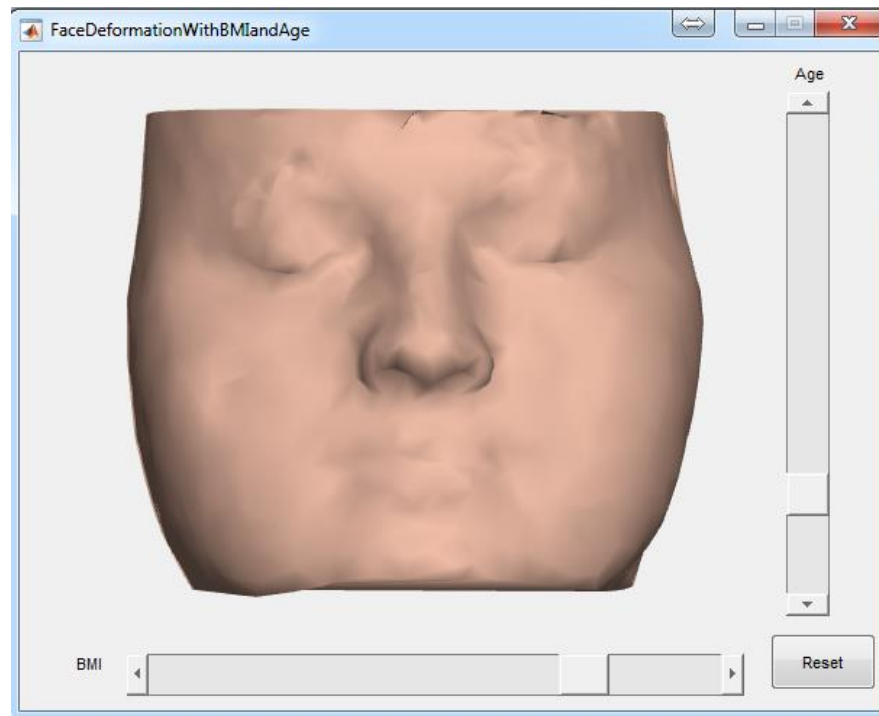
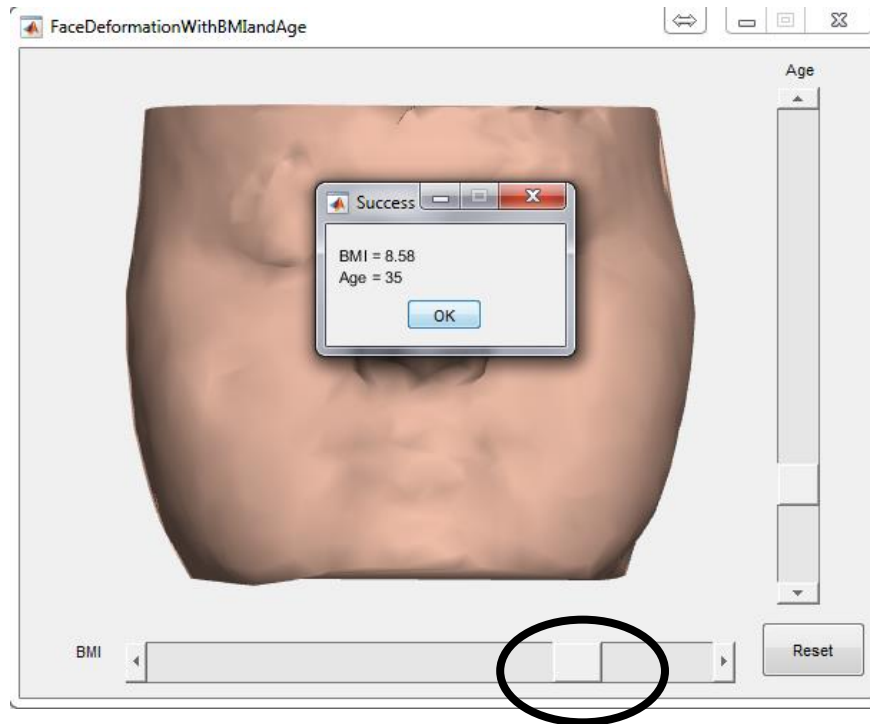


Figure 4-17: BMI change results on Interactive tool. First image: original face with no BMI and age changes. 2nd image: Slider on the bottom moved to the right (highlighted by an oval shape). New age and BMI are displayed in a message box every time slider is moved. 3rd image: New facial appearance with the changed BMI.

4.2.2 Illustration 2

In this illustration the age is changed using the vertical slider bar and the changes are shown below using **Error! Reference source not found.**

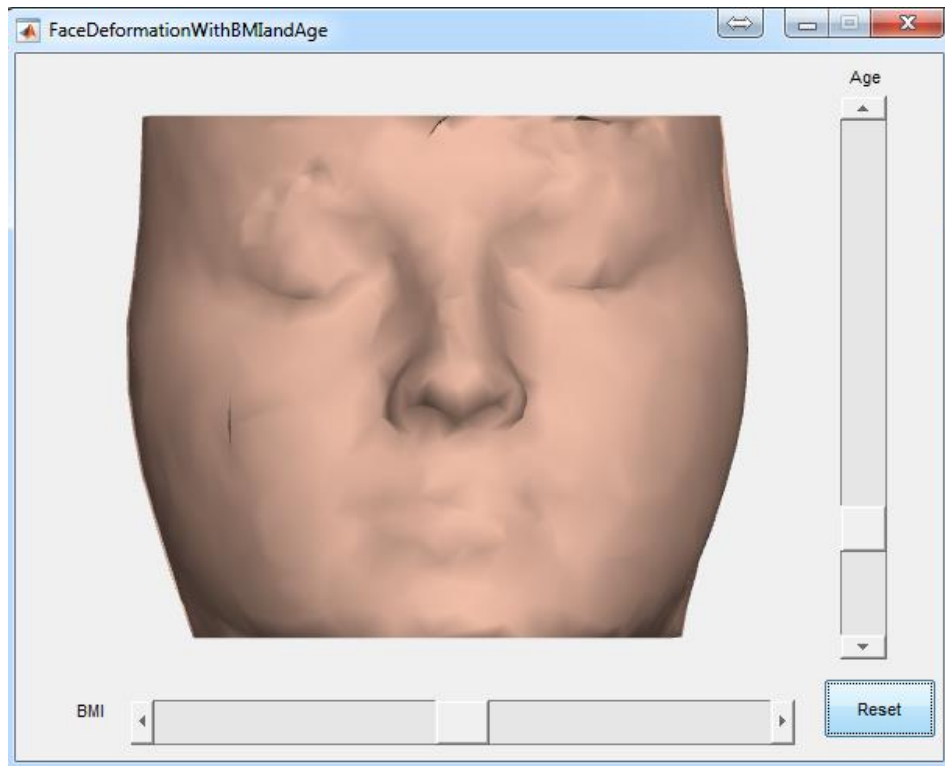


Figure 4.18 continued

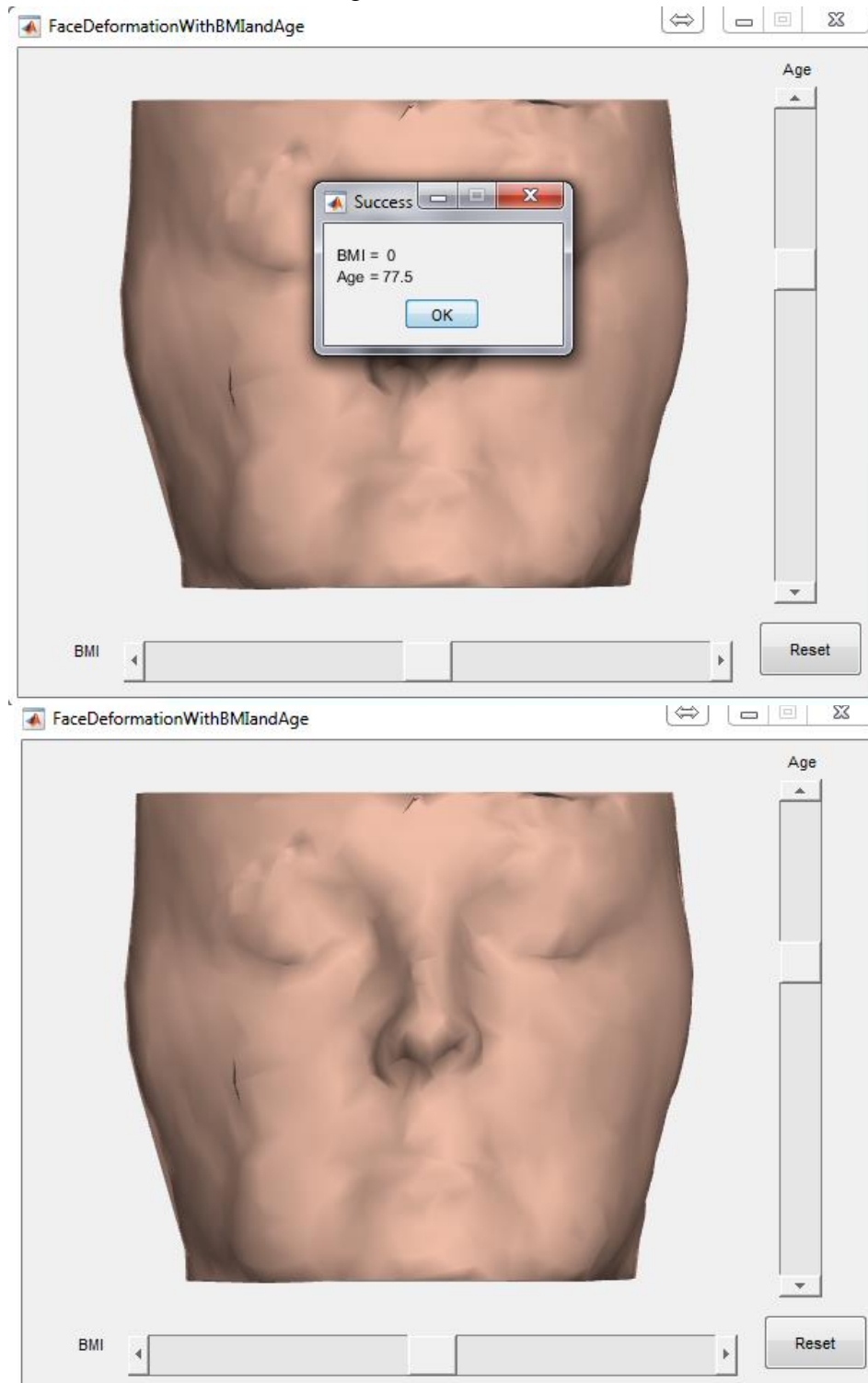


Figure 4-18: Age change results on Interactive tool. First image: original face with no BMI and age changes. 2nd image: Vertical slider on the right has been moved upwards (highlighted by an oval shape). New age and BMI are displayed in a message box every time slider is moved where new age is 77.5 years. 3rd image: New facial appearance with the changed age.

4.2.3 Illustration 3

In this illustration, we change the age and BMI using the horizontal and vertical sliders from the interactive window. The facial changes and appearance once the sliders are moved are illustrated using the below:

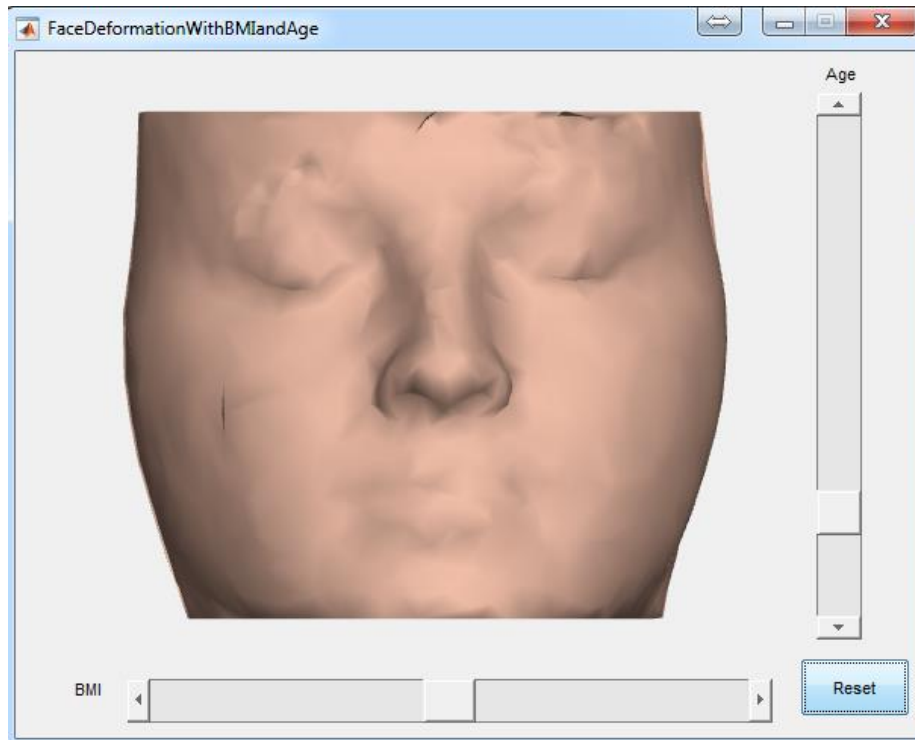


Figure 4.19 continued

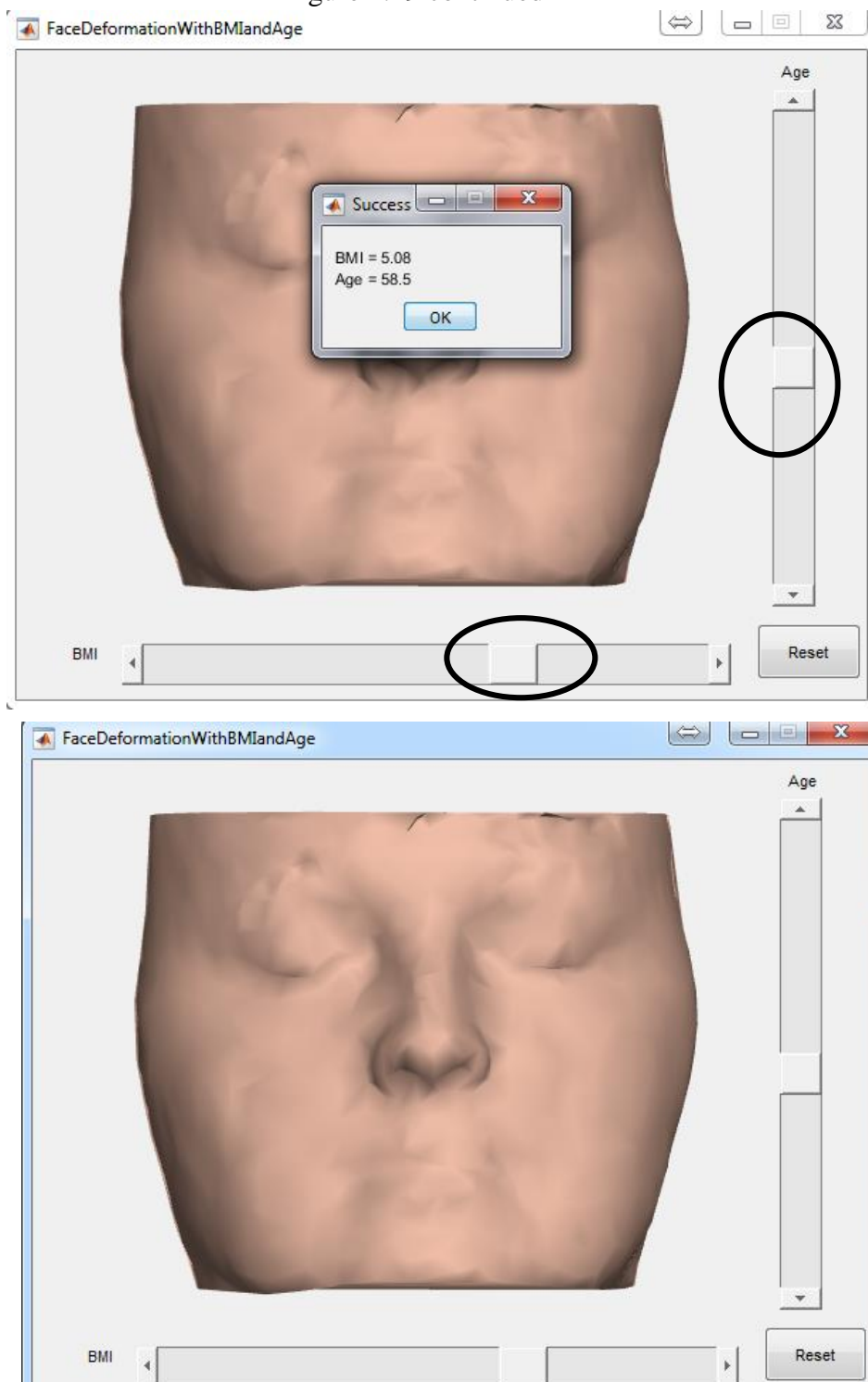


Figure 4-19: Age and BMI change results on Interactive tool. First image: original face with no BMI and age changes. 2nd image: Horizontal slider for BMI is moved to the right changing the BMI to 5.08 and vertical slider on the right has been moved upwards (highlighted by an oval shape) changing the age to 58.5. The new age and BMI are displayed in the message box. 3rd image: New facial appearance with the changed age and BMI is displayed.

5. DISCUSSION

The illustrations, the results from the survey and the reliability tests that are presented above indicates that the system generated is practical for consideration during real scenarios such as forensic face identification. This method could be efficiently used for identifying unknown decomposed bodies with an easy way of changing face appearance by the examiner. The use of such a system would minimize the amount of time it takes using the antiquated reconstruction techniques like sculpting using clay, etc., and mitigate the painstaking process of clay molding.

Many computer-aided facial reconstruction techniques have emerged in the past century but the main feature that separates our work from other existing works is that our methodology is fully automated without human interaction while generating the reconstruction. All the faces with the skull are to be registered and once the registration process is done, the bone model of the test sample can be provided and the results of the facial reconstruction are generated automatically. Another important characteristic of our method is the interactive tool for changing the facial appearance of the predicted face that simplifies the identification by 80% and this tool being useful for any unknown sample. This feature has not been included in any existing works posing as one of our prominent features.

Although there are many uses for this functionality, there are also many ways our present system could be enhanced to make a better Computer-aided Craniofacial Reconstruction technique. Firstly, the dataset that was available and was used to test our functionality has been found to have inconsistent data with missing forehead, chin and in some cases tip of the nose information. Due to data scarcity, we had to use the available data by regulating the information and not considering the complete forehead, excluding the supraglabella region and the lower chin area for all the samples we considered both during training and testing. Due to this reason, the results obtained by our systems could not hold a 100% accuracy. This could be improved by obtaining data with complete head scan, without any inconsistencies throughout the whole sample list.

Secondly, the system requirements that was available for our experimentation was very minimal. The memory constraints were very high and the disk storage space available was less than 16 GB. To compensate for these memory requirements as well as computation time requirements, we reduced the resolution of the meshes by 94%, losing the feature details of the face. This yielded low resolution in the results as well, decreasing the effectiveness of the

functionality. Adding to this, our system was coded using MATLAB which is good for quick prototyping but is not optimal for production versions with fast run times. As performance is key in a real setting, using a better programming language to effectively work this functionality would massively improve the current system. Therefore, high resolutions of data and better programming environment are recommended to enhance the working and expediency of the system.

The face displayed in the interactive tool has shading and lighting applied to it but have no texturing or facial features. The facial features like eyebrows, eyes, eye color, hair color, face color, etc., play a vital role in identification. The CBCT data collected has the color-coded information of the facial features. This color information can be used to learn the patterns and could be used to come up with colored facial features. Addition of these features would eliminate the further confusion during identification and therefore would be a good improvement in future work for more lively and realistic results.

Lastly, the face reconstruction that is been done in the experimentation uses the full skull model for reconstructing the face. One good future development for the experimentation would be to reconstruct the face from partial skull data. When retrieving bodies from crime scenes for identification, it is possible that the body is already disfigured or damaged. The chances of retrieving an intact skull in such circumstances is not high. Therefore, extending the facial reconstruction to work with partial skull model would be a good addition to the present software, considering to extend over all real time scenarios.

6. CONCLUSION

A computer-aided 3D dense facial reconstruction technique has been developed in this research that exhibited promising results both quantitatively and qualitatively. The use of machine learning techniques and various image processing techniques in the study has helped created a distinctive yet very obliging set of features. Starting from the data extraction and pre-processing, the two-step registration and statistical methods usage to create an accurate system for identification. Adding the reduced time complexity from months to minutes, this process has truly shown productivity and throughput improvements. With its ease of usage, this system has been proved to be very compatible to most of the age groups, making it very reliable in a real time environment.

Without limiting to the functionality itself, this system has been rigorously tested. Being one of a kind in validation, this study has gone through extremes for setting up a survey, gathering results which have not only proved valuable but are challenging the golden standards set in this field of research. In the end, this research proved its feasibility and usability by achieving a 100% majority hit rate and a recognition rate of above 74%.

REFERENCES

- Amberg, B., Romdhani, S., & Vetter, T. (2007, 17-22 June 2007). *Optimal Step Nonrigid ICP Algorithms for Surface Registration*. Paper presented at the 2007 IEEE Conference on Computer Vision and Pattern Recognition.
- Berar, M., Desvignes, M., Bailly, G., & Payan, Y. (2005, 15-17 Sept. 2005). *3D statistical facial reconstruction*. Paper presented at the ISPA 2005. Proceedings of the 4th International Symposium on Image and Signal Processing and Analysis, 2005.
- Besl, P. J., & McKay, N. D. (1992). A method for registration of 3-D shapes. *IEEE Transactions on Pattern Analysis and Machine Intelligence*, *14*(2), 239-256. Retrieved from <http://ieeexplore.ieee.org/ielx1/34/3469/00121791.pdf?tp=&arnumber=121791&isnumber=3469>. doi:10.1109/34.121791
- Blanz, V., & Vetter, T. (1999). *A morphable model for the synthesis of 3D faces*. Paper presented at the Proceedings of the 26th annual conference on Computer graphics and interactive techniques.
- Bon-Woo, H., & Seong-Whan, L. (2003). Reconstruction of partially damaged face images based on a morphable face model. *IEEE Transactions on Pattern Analysis and Machine Intelligence*, *25*(3), 365-372. doi:10.1109/tpami.2003.1182099
- Claes, P., Vandermeulen, D., De Greef, S., Willems, G., & Suetens, P. (2006). Statistically Deformable Face Models for Cranio-Facial Reconstruction. *Journal of Computing and Information Technology*, *14*(1), 21-30. doi:10.2498/cit.2006.01.03
- De Greef, S., Claes, P., Vandermeulen, D., Mollemans, W., Suetens, P., & Willems, G. (2006). Large-scale in-vivo Caucasian facial soft tissue thickness database for craniofacial reconstruction. *Forensic Science International*, *159*, S126-S146. doi:10.1016/j.forsciint.2006.02.034
- De Greef, S., & Willems, G. (2005). Three-dimensional cranio-facial reconstruction in forensic identification: latest progress and new tendencies in the 21st century. *J Forensic Sci*, *50*(1), 12-17.
- Liao, Q., Jin, X., & Zeng, W. (2012). Enhancing the symmetry and proportion of 3D face geometry. *IEEE Trans Vis Comput Graph*, *18*(10), 1704-1716. Retrieved from <https://www.ncbi.nlm.nih.gov/pubmed/22291158>. doi:10.1109/TVCG.2012.26
- Manhein, M. H., Listi, G. A., Barsley, R. E., Musselman, R., Barrow, N. E., & Ubelaker, D. H. (2000). In vivo facial tissue depth measurements for children and adults. *J Forensic Sci*, *45*(1), 48-60.
- MathWorks Isosurface. (2016). Isosurface. Retrieved from <https://www.mathworks.com/help/matlab/ref/isosurface.html>
- MathWorks mldivide. (2016). mldivide. Retrieved from <https://www.mathworks.com/help/matlab/ref/mldivide.html>
- National Crime Information Center's (NCIC's). (2018). *2018 NCIC Missing Person and Unidentified Person Statistics*. Retrieved from <https://www.fbi.gov/file-repository/2018-ncic-missing-person-and-unidentified-person-statistics.pdf/view>
- Phillips, V. M., & Smuts, N. A. (1996). Facial reconstruction: Utilization of computerized tomography to measure facial tissue thickness in a mixed racial population. *Forensic Science International*, *83*(1), 51-59. Retrieved from [ISI>://WOS:A1996VT30700006](https://doi.org/10.1016/0379-0738(96)02010-5). doi:Doi 10.1016/0379-0738(96)02010-5

- Shrimpton, S., Daniels, K., de Greef, S., Tilotta, F., Willems, G., Vandermeulen, D., . . . Claes, P. (2014). A spatially-dense regression study of facial form and tissue depth: Towards an interactive tool for craniofacial reconstruction. *Forensic Science International*, 234, 103-110. Retrieved from <Go to ISI>://WOS:000329119100023. doi:10.1016/j.forsciint.2013.10.021
- Sorkine, O., Cohen-Or, D., Lipman, Y., Alexa, M., Rössl, C., & Seidel, H. P. (2004). *Laplacian surface editing*. Paper presented at the Proceedings of the 2004 Eurographics/ACM SIGGRAPH symposium on Geometry processing - SGP '04, Nice, France.
- Subsol, G., & Quatrehomme, G. (2005). Automatic 3D facial reconstruction by feature-based registration of a reference head. In J. G. Clement & M. K. Marks (Eds.), *Computer-Graphic Facial Reconstruction* (pp. 79-101).
- Tedeschi-Oliveira, S. V., Melani, R. F. H., de Almeida, N. H., & de Paiva, L. A. S. (2009). Facial soft tissue thickness of Brazilian adults. *Forensic Science International*, 193(1-3), Pages 127.e121-127.e127. Retrieved from <Go to ISI>://WOS:000272967900020. doi:10.1016/j.forsciint.2009.09.002
- Tu, P., I. Hartley, R., Lorensen, W., Alyassin, A., Gupta, R., & Heier, L. (2005). Face Reconstruction Using Flesh Deformation Modes. In *Computer-graphic Facial Reconstruction* (pp. 145-163).
- Vignal, J., & Schuliar, Y. (2002). *Computer-assisted facial reconstruction. Three years' results and new perspectives*. Paper presented at the Proceedings of the Tenth Meeting of the International Association for Craniofacial Identification.
- Wilkinson, C. (2010). Facial reconstruction—anatomical art or artistic anatomy? *Journal of Anatomy*, 216(2), 235-250. Retrieved from <https://www.ncbi.nlm.nih.gov/pmc/articles/PMC2815945/pdf/joa0216-0235.pdf>.
- Wilkinson, C., Rynn, C., Peters, H., Taister, M., Kau, C. H., & Richmond, S. (2006). A blind accuracy assessment of computer-modeled forensic facial reconstruction using computed tomography data from live subjects. *Forensic Sci Med Pathol*, 2(3), 179-187. Retrieved from <https://link.springer.com/article/10.1007%2Fs12024-006-0007-9>. doi:10.1007/s12024-006-0007-9
- Zaki, M. J., & Meira, W., Jr. (2014). *Data Mining and Analysis: Fundamental Concepts and Algorithms*: Cambridge University Press.
- Zhao, H., Jin, X., Huang, X., Chai, M., & Zhou, K. (2018). Parametric Reshaping of Portrait Images for Weight-change. *IEEE Comput Graph Appl*, 38(1), 77-90. Retrieved from <https://www.ncbi.nlm.nih.gov/pubmed/29535075>. doi:10.1109/MCG.2018.011461529